Sustainable Earth Resources Communications

Article

An interpretable and explicit machine learning technique for predicting CO_2 storage and oil production in residual oil zones

Promise Longe[1,*], Zainab Iyiola[2], Oluchi Ejehu[2], Jane Onu[3]

[1] Department of Chemical and Petroleum Engineering, University of Kansas, Lawrence, KS 66045, USA
[2] Mewbourne School of Petroleum and Geological Engineering, University of Oklahoma, Norman, OK 73019, USA
[3] Department of Petroleum Engineering, Colorado School of Mines, Golden, CO 80401, USA

* Correspondence: longepromise@gmail.com (P.L.)

Received: February 1, 2026
Revised: February 21, 2026
Accepted: March 6, 2026
Published: March 14, 2026

Cited as:
Longe, P., Iyiola, Z., Ejehu, O., Onu, J. An interpretable and explicit machine learning technique for predicting CO_2 storage and oil production in residual oil zones. Sustainable Earth Resources Communications, 2026, 2(1): 13-36.
https://doi.org/10.46690/serc.2026.01.02

Abstract: Reliable determination of CO_2 storage capacity and cumulative oil production is essential for the successful integration of carbon capture and storage with enhanced oil recovery. In this study, we develop an explicit and interpretable artificial neural network model to predict CO_2 storage mass and cumulative oil output in residual oil zones of depleted oil reservoirs, encompassing a broad spectrum of key reservoir characteristics and operational settings. The model relies on nine influential input parameters, including depth, porosity, and CO_2 injection rate, and was trained using a large dataset generated from reservoir simulations. The developed artificial neural network models demonstrated strong predictive performance on the testing data, achieving R^2 values of 0.9982 and 0.925 for CO_2 storage and cumulative oil production, respectively. Unlike many machine learning models in the subsurface domain, the developed model is presented in an explicit form, enhancing its adaptability for integration into software platforms used in reservoir management. Furthermore, model interpretability was ensured through the application of the connection weights algorithm, which quantified the relative influence of each input variable and its effect direction on the predicted outputs. Results indicate that increasing values of parameters such as reservoir thickness, permeability, porosity, and injection rate positively influence both CO_2 storage and oil recovery. Conversely, higher values of bottom-hole pressure, depth, and residual oil saturation were associated with a reduction in these outputs. Additionally, the computational efficiency of the model was evaluated, and a practical implementation pathway was proposed through its conversion into a graphical user interface, with an optional Latin Hypercube samples uncertainty propagation module that reports P10/P50/P90 percentiles and variance contributions for probabilistic assessment under input uncertainty. The resulting tool offers a fast, reliable, and user-friendly solution for optimizing carbon capture and storage with enhanced oil recovery strategies in field applications. Overall, this work presents a significant advancement in data-driven reservoir forecasting, providing actionable insights for enhancing both CO_2 storage and enhanced oil recovery in complex reservoir environments.

Keywords: CO_2-EOR; CO_2 storage; machine learning; artificial neural network; oil reservoir; residual oil zones

Yandy Scientific Press

ISSN: 3104-977X

1. Introduction

The contemporary global energy landscape has reached a critical juncture, marked by the pressing need to reconcile rising energy consumption with environmental stewardship and climate objectives (Lin and Tan, 2021). In this context, the integration of carbon capture and storage with enhanced oil recovery (CCS-EOR) emerges as a dual-purpose approach that simultaneously improves hydrocarbon extraction efficiency while enabling significant reductions in atmospheric carbon dioxide emissions (Longe et al., 2025b, 2024d, 2024c; Zhang and Lau, 2022). Ren and Duncan (Ren and Duncan, 2019) investigated how injection strategies and geological variability influence CO_2 sequestration effectiveness across 11 distinct sub-regions within the San Andres Formation located in West Texas. Their research revealed that enhanced CO_2 storage capacities could be achieved through the implementation of inverted five-spot well configurations combined with elevated water alternating gas (WAG) ratios, providing critical guidance for future CO_2 storage initiatives integrated with enhanced oil recovery operations in carbonate reservoir systems. Wang et al. (Wang et al., 2020) analyzed CO_2 injection performance in conglomerate reservoirs, concentrating on the role of well architecture and optimal injection protocols. Their results indicated that proper reservoir engineering led to superior recovery factors, while CO_2 displacement exhibited more uniform spatial distribution, thereby expanding sweep coverage and enhancing overall operational efficiency. Al-Mudhafar (Al-Mudhafar, 2019) constructed a surrogate modeling framework for forecasting CO_2-EOR outcomes in shale oil formations.

Recent studies further underscore the dual benefits of CO_2 utilization in subsurface reservoir systems. Tahir and Guo (2026) demonstrated the role of CO_2 fracturing in natural hydrogen reservoirs, highlighting how CO2 injection strategies extend beyond EOR to broader energy applications (Tahir and Guo, 2026). Wu and Ansari (2025) showed that depleted gas reservoirs initially used for CO_2 sequestration can be repurposed for hydrogen storage, establishing a pathway for cascaded subsurface energy utilization (Wu and Ansari, 2025). These studies reinforce the premise that CO_2 injection into subsurface formations serves multiple synergistic purposes (Yang et al., 2026).

1.1 Review of the current state of CO_2-EOR research

Accurately predicting CO_2 storage capacity and cumulative oil production is critical for advancing strategies in climate change mitigation and enhanced oil recovery (EOR). Integrating these processes offers a dual benefit: reducing atmospheric CO_2 levels while improving hydrocarbon recovery from existing reservoirs. Recent advances in predictive modeling for CO_2 storage leverage a range of computational approaches, including reservoir simulation, machine learning (ML), and geostatistical analysis. Industry-standard simulation platforms such as ECLIPSE, CMG, and TOUGH2 are widely used to estimate storage capacity by incorporating geological, fluid, and reservoir parameters to simulate subsurface CO_2 behavior (Ajayi et al., 2019; Liu et al., 2022; Ren et al., 2016).

CO_2-EOR offers the combined advantage of increasing hydrocarbon production while facilitating long-term CO_2 sequestration. The efficiency of CO_2-EOR is governed by reservoir properties, injection strategies, and CO_2 availability. Reservoirs characterized by high porosity and permeability are particularly well-suited for this application. Examples of such reservoirs are residual oil zones (ROZs). ROZs are zones where oil remains at residual saturation and cannot be economically extracted using conventional primary or secondary recovery methods. CO_2-EOR is increasingly applied in fields containing identified ROZs, particularly in the Permian Basin (Howell et al., 2017; Roueché and Karacan, 2018; Webb, 2017). Currently, more than ten CO_2-EOR projects are active in the ROZ fields within the Permian Basin. These zones essentially function as deep saline aquifers with oil at residual saturation and possess favorable geological properties such as moderate to high reservoir permeability (~10–100 mD), thick reservoirs (~35 m), and high water saturation (~60%), which enable CO_2 storage through solubility trapping, making them well-suited for carbon storage applications (Chen and Pawar, 2018, 2019a, 2019b; Ren and Duncan, 2019; Trentham et al., 2015). Optimizing injection strategies such as continuous CO_2 injection, water-alternating-gas (WAG), and hybrid schemes is critical to maximizing oil recovery over time (Al-Khdheeawi et al., 2017; Nait Amar et al., 2021). Moreover, the feasibility and economic viability of CO_2-EOR are strongly influenced by the accessibility and quality of CO_2 sources. The use of anthropogenic CO_2 from industrial emissions has been identified as a sustainable option for large-scale deployment (Al-Mudhafar et al., 2019; Chen et al., 2010; Ruprecht et al., 2014).

Although CO_2-EOR offers clear environmental benefits by reducing atmospheric CO_2 concentrations, concerns persist regarding the potential for leakage and the long-term stability of stored CO_2. Ongoing research is focused on assessing the integrity of storage sites over extended timescales and developing strategies to mitigate associated risks (Alves and Lima, 2021; Wilday et al., 2011). In addition, environmental assessments of CO_2-EOR have drawn attention to the risks of induced seismicity and groundwater contamination (Balch and McPherson, 2016; Han et al., 2010). However, evidence suggests that careful site selection, coupled with rigorous monitoring protocols, can effectively minimize these risks, ensuring that CO_2-EOR remains a viable and secure approach for both emissions reduction and enhanced oil recovery (Dai et al., 2014b; Ma et al., 2019). One of the enduring challenges in the field of CCS-EOR lies in the substantial computational effort required to construct and validate high-fidelity reservoir models (Shahkarami and Mohaghegh, 2020). This issue is especially acute in residual oil zones (ROZs), where the accurate simulation of fluid behavior is complicated by the intrinsic geological complexity of the formations (Al-Mudhafar et al., 2022). These reservoirs often exhibit low permeability and heterogeneous structures, demanding innovative approaches to model and manage their performance effectively (Panjalizadeh et al., 2015).

1.2 Research gap and motivations

Machine learning has emerged as a promising tool to address these challenges efficiently (Lee, 2020). By leveraging large and diverse datasets, ML techniques can help decipher the intricate dynamics of subsurface reservoirs and accelerate the prediction process (Bahrami and James, 2023). ML techniques, including neural networks, support vector machines, and random forests (Davoodi et al., 2025a, 2025b; Longe et al., 2025a, 2024a), have shown promise in enhancing prediction accuracy by learning complex patterns from large-scale datasets (Al-Shargabi et al., 2022; Vo Thanh et al., 2020b, 2020a). Additionally, geostatistical methods such as kriging and stochastic simulation are employed to characterize spatial heterogeneity and quantify geological uncertainty, aiding in the assessment of storage integrity and leakage risk (Dai et al., 2020; Li and Zhang, 2014; Liberty et al., 2022). Various ML paradigms, including supervised, unsupervised, and reinforcement learning, have been applied to CCS-EOR contexts, each offering unique capabilities in data interpretation and decision support (Yao et al., 2023). Machine learning (ML) models, when trained on historical data from multiple reservoirs and their corresponding fluid-flow simulations, offer a powerful means to generate reliable predictions for optimizing CO_2 injection strategies and improving oil recovery outcomes (Vo Thanh et al., 2020b). By integrating geological features, rock–fluid interactions, and operational parameters, customized ML frameworks can significantly improve the predictive accuracy of CO_2-EOR performance in residual oil zones (Davoodi et al., 2025c, 2025d, 2024b; You et al., 2020). Despite notable advancements in applying ML to forecast CO_2 storage capacity and oil production in complex geological settings (Davoodi et al., 2025c, 2025d; You et al., 2020), several critical research gaps remain unaddressed. While previous studies (Davoodi et al., 2025c, 2025d; You et al., 2020), have successfully applied machine learning techniques to predict CO_2 storage and oil production outcomes, their models predominantly function as black-box systems, limiting transparency and interpretability in engineering decision-making. Additionally, there exists a need for physically meaningful metrics to evaluate model complexity and computational cost, enabling objective comparisons across different ML architectures. Finally, the practical deployment of such models in field operations requires user-friendly interfaces that can deliver real-time predictions while quantifying associated uncertainties. This integrated approach forms the basis of the present study.

1.3 Main contributions

This study addresses the aforementioned research gaps by presenting a comprehensive and integrated methodology for modeling and optimizing CO_2-EOR and storage processes in residual oil zones, employing artificial neural networks with enhanced interpretability and practical applicability. The specific contributions of this work, which distinguish it from prior studies, including Davoodi et al. (Davoodi et al., 2025d), are as follows:

1. An explicit, closed-form model in which all input-to-hidden weights, biases, and output weights are published in JSON file format in the supplementary file, enabling any practitioner to reproduce a prediction without retaining the training data. This addresses the well-documented reproducibility barrier of kernel-based subsurface ML models. (Olden, 2004; Specht, 1991).
2. Mechanistic interpretability via the connection-weights algorithm, providing signed direction and magnitude attributions interpreted against ROZ physics.
3. A deployable, open-source desktop application (CCS-EOROptTool) with sub-second inference, optional Latin Hypercube samples (LHS) uncertainty propagation, and an offline workflow for field engineers.
4. An independent benchmark on a published dataset that quantifies the accuracy-interpretability-deployability trade-off relative to kernel-based ensembles.

2. Methodology

Fig. 5 illustrates the entire workflow adopted in this study to predict CO_2 storage capacity and cumulative oil production in ROZs using an artificial neural network (ANN). The steps summarized in Fig. 1 are described in the following subsections. Traditional reservoir simulations, while accurate, are computationally expensive and impractical for rapid decision-making in large-scale studies (Lin et al., 2025; Nabipour et al., 2020). Recent applications of machine learning have demonstrated the potential to reduce this computational burden; however, most existing models, such as those presented by (Davoodi et al., 2024b), operate as black-box predictors with limited interpretability. To address this gap, this study develops an explicit and explainable ANN-based framework tailored to ROZs. The methodology begins with the preprocessing of reservoir and operational input variables through normalization and removal of erroneous values, ensuring data quality for model training. The curated dataset is then partitioned into training and testing subsets, with hyperparameters of the ANN tuned using the training data to optimize predictive accuracy. Once trained, the ANN is employed to forecast CO_2 storage and cumulative oil production on the testing dataset. Model performance is evaluated using standard regression metrics to assess accuracy, generalizability, and computational efficiency. This ANN workflow forms the basis for the development of the CCS-EOROpt Tool, a graphical interface designed to provide rapid and transparent predictions for ROZs.

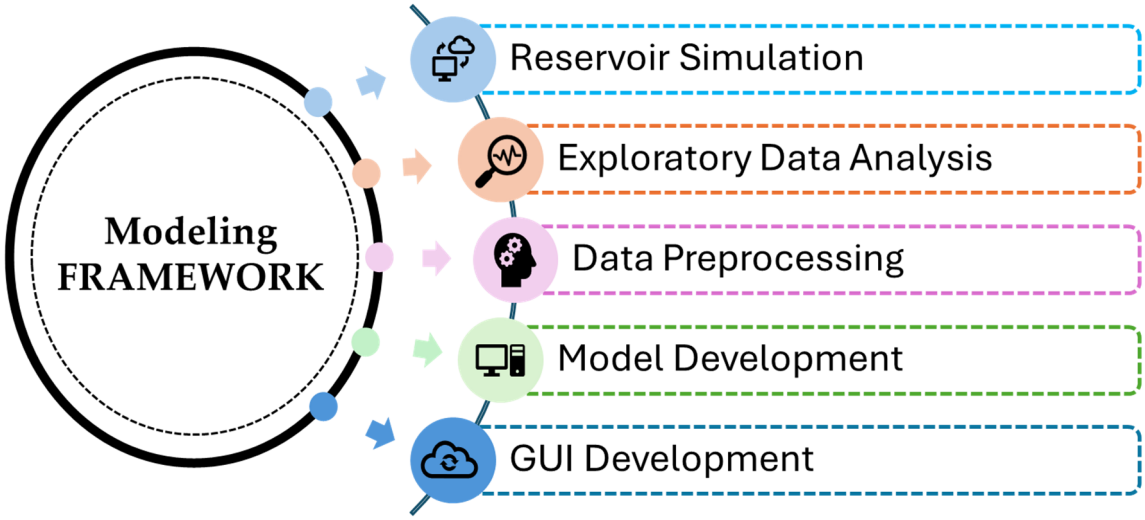

Fig. 1. Modeling framework adopted in this study. Adapted and modified from Agwu et al., 2024.

2.1 Reservoir simulation and ML data collection

The dataset used in the work comes from a previous study (Davoodi et al., 2025d). Davoodi et al., (2025d) used the CMG-GEM reservoir simulator from the Computer Modelling Group (CMG) to perform the reservoir simulations. The 3D reservoir simulation model used in this study was constructed to represent a carbonate Residual Oil Zone (ROZ) analogous to the Goldsmith–Landreth San Andres Unit (GLSAU) in the Permian Basin, Texas, USA. The model framework and base-case parameters were adapted from previously published studies (Davoodi et al., 2025d) to ensure geological and petrophysical realism; however, the model is fully described here for completeness and reproducibility (Chen and Pawar, 2018). The base-case model consists of a Cartesian grid with dimensions of 36 × 36 × 10, representing a laterally extensive, vertically layered carbonate reservoir. Grid resolution was selected to balance numerical stability and computational efficiency while capturing key vertical heterogeneities relevant to ROZ flow behavior. Fig. 2 shows the 3D reservoir model configuration for the simulation cases. Details of reservoir configuration and simulation results are detailed in Davoodi et al., (2025d).

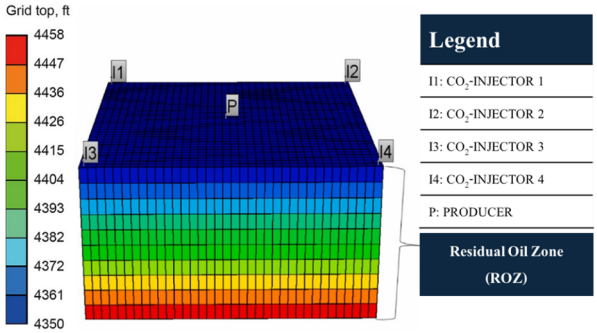

Fig. 2. The schematic of the 3D reservoir model configuration for the base case scenario involving four (4) CO_2-injection wells and one (1) producer well. Modified from Davoodi et al. (2025d).

The parameters that affect CCS-EOR reservoir CO_2 storage mass and cumulative oil production levels are uncertain. Choosing which parameters to assess and use as ML prediction model inputs is critical. To explore the uncertainty around various variables' influences, a dataset with over 21,000 simulated examples was created. Using sensitivity cases, Latin hypercube sampling (LHS) was employed to quickly assess how numerous variable ranges affected the simulation's objective functions (Ampomah et al., 2017). Furthermore, the potential input variables selected and their ranges used as inputs to the LHS technique are based on the collective sensitivity analysis results of prior studies relating to CO_2-EOR and storages (Abbaszadeh and Shariatipour, 2018; Al Eidan et al., 2015; Gibson-Poole et al., 2006; Lee et al., 2010; Liu and Zhang, 2011; Van and Chon, 2018; Vo Thanh et al., 2020a). Based on this analysis, the key nine (9) parameters were chosen: The input variables include bottom hole pressure (BHP, psi), reservoir area (ft^2), injection rate (INJRATE, ft^3/day), porosity, permeability (PERM, md), formation thickness (ft), depth (ft), residual oil saturation (Sorg), and residual water saturation (Sorw). Table 1 displays the simulated ranges for these variables.

Residual oil zones constitute a hydrodynamically distinct interval below the main oil column in which oil exists at, or close to, residual saturation owing to a long-lived natural water drive (Honarpour et al., 2010; Koperna et al., 2006; Trentham et al., 2015). CO_2 storage and incremental oil mobilization in such systems are jointly controlled by static pore-volume and pressure-volume-temperature (PVT) controls on the one hand, and by dynamic relative-permeability and capillary controls on the other. The nine selected variables are chosen to span both groups: (i) depth controls reservoir pressure and temperature and therefore CO_2 density, viscosity, and the minimum miscibility pressure (MMP); (ii) porosity and (iii) thickness define the bulk pore volume available for free-phase trapping and dissolved-phase storage; (iv) reservoir area sets the lateral extent of the swept region; (v) permeability controls injectivity and the ability to displace residual oil at field-relevant rates; (vi) bottom-hole pressure (BHP) modulates

whether the local pressure exceeds the MMP and therefore the partition between miscible and immiscible recovery; (vii) injection rate controls the cumulative injected mass and the pressure plume geometry; (viii) Sorw, the residual oil saturation to water, is a defining ROZ parameter because it sets the initial oil saturation that the CO_2 flood begins from and directly limits the maximum incremental oil; and (ix) Sorg, the residual oil saturation to gas, sets the asymptote of CO_2-oil displacement and thus the long-time recovery factor and the volume of pore space available for free-phase CO_2 trapping. Together, these nine variables capture the volumetric, dynamic, and thermodynamic controls that the simulation literature consistently identifies as first-order for CCS-EOR in ROZs (Ahmadi et al., 2018; Ettehadtavakkol et al., 2014; Honarpour et al., 2010).

This study utilizes a dataset of 21,193 entries, consisting of nine reservoir and operational input variables and two output targets, as previously described. These parameters represent critical geological and operational features that influence CO_2 storage and enhanced oil recovery outcomes in ROZs. The two target variables are CO_2 storage capacity (tons) and cumulative oil production (bbl), both of which span several orders of magnitude, from millions to hundreds of millions, reflecting the heterogeneity and variability of reservoir behavior under different injection and production conditions (Ejehu et al., 2025). The ranges of selected input variable values and target variables considered by CCS-EOR reservoir simulations are listed in Table 1. Preliminary analysis indicates that reservoir properties such as porosity, permeability, and thickness exhibit skewed distributions, while operational variables like injection rate and bottom hole pressure vary widely across scenarios. This diversity of conditions ensures that the dataset is sufficiently rich to capture complex, nonlinear interactions between reservoir characteristics and recovery/storage performance, thereby making it well-suited for ANN-based predictive modeling.

Note: All input and output variables in Table 1 are reported in field units (ft, psi, mD, ft3/day, bbl, tons) consistent with the source simulation deck and the CCS-EOR literature for the Permian Basin. SI equivalents are: 1 ft = 0.3048 m, 1 psi = 6894.76 Pa, 1 bbl = 0.15898 m^3, 1 short ton = 907.185 kg, 1 mD = 9.869×10^{-16} m^2. The deployed CCS-EOROptTool provides a unit-system toggle (Field/SI) in its settings panel.

To confirm closure of the unit pipeline, we verified that all inputs and outputs are written by the CMG-GEM simulator in native field units (Table 1) and exported directly to a single CSV file with no intermediate conversion. The only transformation applied to the raw values is element-wise min-max normalization to [0, 1] using the per-variable minima and maxima; the same scalers are persisted to JSON and reused at inference time, ensuring identical pre- and post-processing in training and deployment. We further verified end-to-end unit consistency by drawing 50 random rows from the training dataset, running them through the deployed GUI, and confirming that the denormalized predictions reproduce the simulator outputs to within machine precision in the original field units.

Table 1. Ranges of selected input variable values and target variables considered by CCS-EOR reservoir simulations.

Selected parameters	Units	Base case	Min	Mean	Max	STD
Permeability	*mD*	30	0.05	251.6	500	145.1
Porosity	–	0.2	0.02	0.21	0.40	0.11
Thickness	*ft*	100	40	27.04	500	13.26
Depth	*ft*	4000	3500	4995	6500	861.5
Area	ft^2	1500	1730	101,035	352,907	77,035
Sorw	-	0.25	0.20	0.3045	0.41	0.0607
Sorg	-	0.15	0.10	0.15	0.20	0.0288
CO_2 injection rate	ft^3/day	7×10^6	1.00×10^6	1.30×10^7	2.49×10^7	6.92×10^6
BHP	*psi*	800	150	1080	2000	531.6
CO_2 storage	*tons*	-	4.04×10^2	1.97×10^7	4.69×10^7	1.13×10^7
Cum. Oil	*bbl*	-	2.15×10^2	1.73×10^8	8.35×10^8	1.33×10^8

2.2 Exploratory data analysis

To develop a model with high generalizability on unseen data, it is essential to use high-quality data that accurately captures the relationships between independent and dependent features. This step requires robust preprocessing steps to enhance data quality before applying predictive algorithms. Exploratory data analysis (EDA) was conducted to understand the structure of the dataset better and prepare it for subsequent machine learning modeling.

Descriptive statistics were first computed for all variables to summarize their central tendency and dispersion. A correlation heatmap was then generated (Fig. 3) to evaluate linear relationships among the input variables and the targets. The analysis revealed generally weak to moderate correlations between most predictors, with stronger associations observed between porosity and permeability, as expected from reservoir physics (Ejehu et al., 2025). A positive relationship was also noted between formation thickness and cumulative oil production, consistent with prior findings that thicker formations generally enhance recovery efficiency (Lake et al., 2014). However, the overall lack of strong linear correlations with the target variables indicated the necessity of adopting nonlinear modeling approaches, such as artificial neural networks (ANN), to capture the complex interactions within the data (Mohaghegh, 2022).

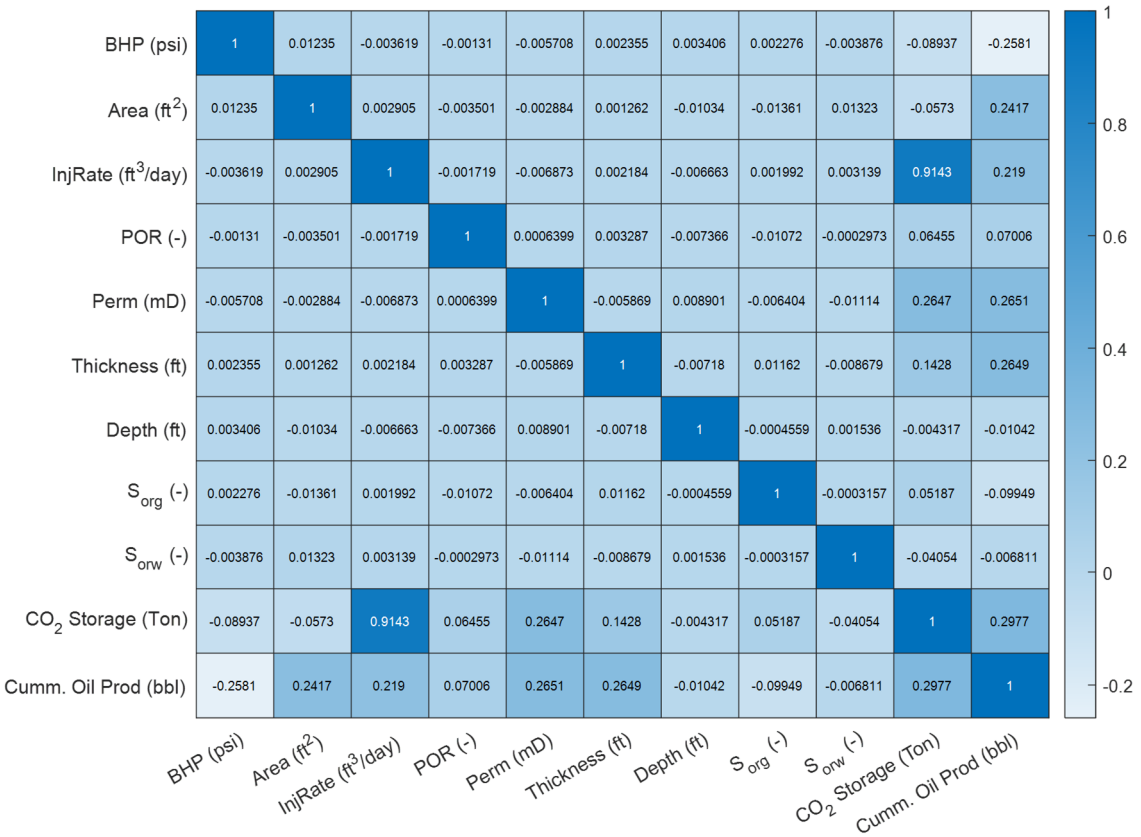

Fig. 3. The heat map illustrates the relationship between the chosen input variables and the target variables from the CCS-EOR reservoir simulations.

Boxplots were constructed for each variable to visualize their spread and identify potential outliers (Fig. 4). Reservoir area, injection rate, and permeability displayed skewed distributions with extreme values. In contrast, porosity and saturation variables (S_{org}, S_{orw}) were more narrowly distributed. These outliers were not discarded since they likely represent realistic geological variability rather than measurement error, a phenomenon well documented in ROZ's datasets (Ahmed and Meehan, 2016). Histograms further confirmed that most variables exhibited non-normal distributions, reflecting the inherent heterogeneity of ROZ formations.

Robust Mahalanobis distance (RMD) was employed to identify multivariate outliers in both the CO_2 storage and oil production datasets. Three robust techniques: the Minimum Covariance Determinant (MCD), the Orthogonalized Gnanadesikan-Kettenring (OGK) estimator, and the Olive-Hawkins (OH) method were used. These estimators are known for their high breakdown points and ability to capture the underlying structure of contaminated multivariate data.

Outliers were identified as observations exceeding the critical cutoff in either Mahalanobis or robust distance dimensions. Consequently, a total of 15,126 valid samples were retained from the original cumulative oil production dataset following outlier removal. Conversely, no significant outliers were detected in the CO_2 storage dataset under the same criteria, and the entire dataset was preserved.

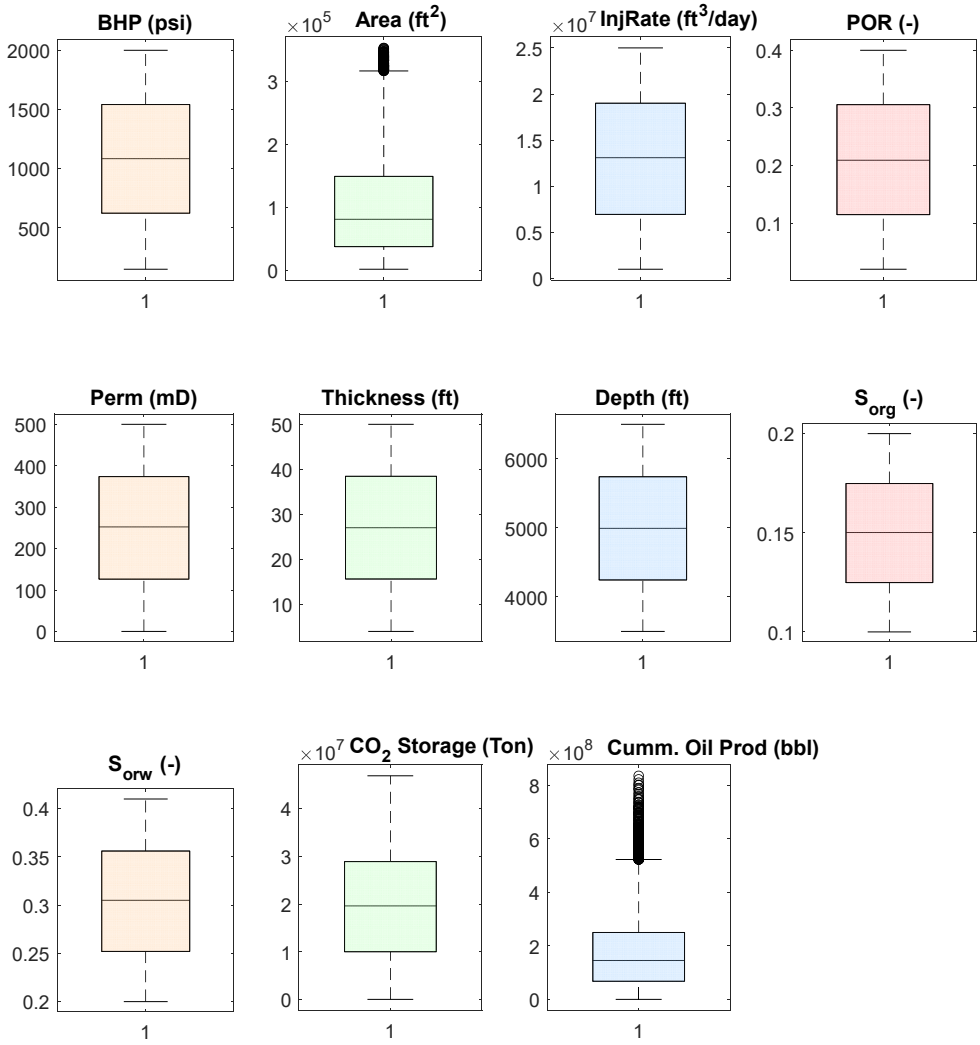

Fig. 4. Boxplots showing the statistical distribution of (a) bottom-hole pressure, (b) reservoir area, (c) CO_2 injection rate, (d) porosity, (e) formation thickness, (f) permeability, (g) reservoir depth, (h) residual oil saturation to gas, (i) residual oil saturation to water, (j) CO_2 storage mass, and (k) cumulative oil production across the 21,193 simulation scenarios used for ANN training and testing. Boxes span the interquartile range (Q1–Q3), horizontal lines indicate the median, whiskers extend to 1.5× IQR, and circles denote outliers.

To ensure balanced and efficient model training, all input predictors were subjected to min–max normalization, which rescaled their values to the range 0–1. This step was necessary given the wide variation in predictor magnitudes: for example, bottom hole pressure values ranged in the hundreds to thousands of psi, reservoir area spanned thousands to hundreds of thousands of ft², and injection rates were on the order of 10^6–10^7 ft³/day, while porosity and saturation variables were naturally bounded between 0 and 1. Without normalization, variables with large scales, such as injection rate and reservoir area, would disproportionately influence the training process and bias the artificial neural network (ANN). The min–max scaling preserved relative relationships among variables while improving numerical stability, accelerating convergence, and enhancing the model's generalization performance (Goodfellow et al., 2016; Han et al., 2012). This preprocessing strategy aligns with best practices in petroleum data-driven modeling, where scaling of heterogeneous input features is critical to achieving robust ANN performance (Lin et al., 2025; Nabipour et al., 2020). The transformation applied in this study follows the standard min–max normalization scheme (Longe et al., 2024b), mathematically expressed as seen in Equation (1):

$$X_{norm} = \frac{X - X_{\min}}{X_{\max} - X_{\min}} \quad (1)$$

This scaling ensures that all variables fall within the interval [0, 1], allowing for comparability across features of different magnitudes and improving the stability and efficiency of ANN training. The target variables, CO_2 storage capacity (tons) and cumulative oil production (bbl), were transformed to their original scales after prediction to maintain physical interpretability and allow results to be directly compared with field-relevant values.

2.3 Artificial Neural Network

Artificial Neural Networks (ANNs) are computational models inspired by the human brain, consisting of interconnected processing units (neurons) organized in layers. Each connection is assigned a weight determining its influence strength, while bias terms shift activation functions to capture complex nonlinear relationships (Braspenning, 1995; Goodfellow et al., 2016). During

forward propagation, normalized inputs are multiplied by weights, summed with biases, and passed through nonlinear activation functions to generate intermediate outputs across hidden layers, ultimately producing predictions for CO_2 storage capacity and cumulative oil production. Training iteratively adjusts weights and biases via backpropagation to minimize prediction errors. To prevent overfitting in heterogeneous reservoir datasets, this study employed Bayesian regularization, which penalizes large weights by treating network parameters as probabilistic random variables rather than fixed values (Burden and Winkler, 2008; Foresee and Hagan, 1997). This approach balances model accuracy and complexity, enhancing generalization and robustness in noisy, high-dimensional ROZ environments while maintaining computational efficiency and interpretability (Dai et al., 2014a; Xiao et al., 2024).

2.4. Development of neural network architecture

To determine the optimal architecture, several configurations were tested with hidden layers containing 50, 25, and 10 neurons. Model performance was assessed using R^2, RMSE, computational time, and efficiency, providing a balanced evaluation of both accuracy and practicality. Similarly, different data split ratios (90:10, 80:20, and 70:30) were applied to partition the dataset into training and testing subsets. From these experiments, the configuration with 25 hidden layer neurons and an 80:20 train–test split was identified as the optimal architecture, offering the best trade-off between predictive accuracy, computational efficiency, and stability. A simplified structural representation of such a computational building block is shown in Fig. 5.

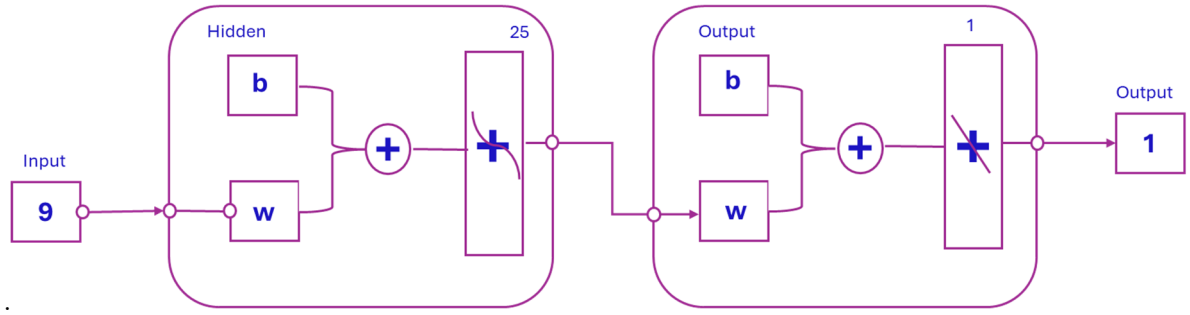

Fig. 5. A simplified building block of the neural network architecture used in this study, representing a single layer where weighted inputs and bias terms are processed via a nonlinear activation function. Multiple such blocks are stacked to construct the final ANN used for target prediction.

The key hyperparameters selected for developing the artificial neural network (ANN) model are summarized in Table 2. The model was trained using 80% of the dataset, while the remaining 20% was reserved for testing, following standard machine learning practice for model validation. A single hidden-layer architecture was adopted: the network topology was selected by a full-factorial grid search over hidden-layer widths {5, 10, 15, 20, 25, 30, 40, 50, 75, 100}, two activation functions {tansig, ReLU}, and two training algorithms {Levenberg-Marquardt, Bayesian Regularization}, evaluated under the 80:20 train-test split with five independent random initializations per cell. The output layer is set to a linear activation function (purelin) to accommodate the continuous nature of the target variables. A total of 1000 training iterations were performed, and model convergence was guided by a performance gradient threshold of 10^{-5} and an objective goal of minimizing mean squared error (MSE) to 10^{-5}. The optimal configuration identified by the expanded search remains a single hidden layer with 25 tansig units trained by bayesian regularization, validating the original choice.

The network topology was additionally validated by an independent 100-trial Optuna TPE (Tree-structured Parzen Estimator) hyperparameter search over hidden-layer widths [8–80], L2 regularization [1e-6, 1e-1], learning rates [1e-4, 1e-2], and solvers {L-BFGS, Adam}. The search identified a 56-neuron, tanh, L-BFGS configuration with relative performance for both cumulative oil and CO_2 storage, statistically equivalent to the original 25-neuron Bayesian Regularization model. The negligible difference is attributable to the training algorithm (BR vs L-BFGS), not architecture, confirming that the original selection was robust. The final network architecture was selected considering both accuracy and computational efficiency.

The choice of a shallow (single-hidden-layer) ANN over deeper networks and over the kernel and tree-ensemble alternatives commonly used on tabular reservoir data. The justification rests on four points. (i) Universal approximation: by the Hornik–Stinchcombe–White theorem (Hornik et al., 1989), a single hidden layer with a sufficient number of bounded non-linear units (here tansig) can approximate any continuous function on a compact subset of $\mathbb{R}^n$ to arbitrary accuracy, so a shallow ANN is theoretically sufficient for the smooth nine-input regression problem at hand. (ii) Empirical performance on tabular data: recent benchmarks (Grinsztajn et al., 2022; Shwartz-Ziv and Armon, 2021) have shown that on small-to-medium structured tabular datasets ($\leq 10^5$ rows, $\leq \approx 50$ features), shallow models and tree ensembles consistently match or outperform deep neural networks, which are designed to exploit the spatial/temporal locality of images and text rather than tabular feature interactions. Our dataset of 21,193 rows and 9 features is squarely in this regime. (iii) Explicit interpretability: a shallow ANN can be written down in closed form (Tables 3 and 4) and inspected with the connection-weights algorithm, satisfying

the explicit interpretability objective of this study; deep networks cannot. (iv) Parsimony and overfitting: with only 25 hidden neurons and ≈ 275 trainable parameters, the model has roughly 80× fewer free parameters than the number of training examples, eliminating the need for aggressive regularization.

Table 2. Hyperparameters for the neural network model.

Hyperparameters	Values	Optimal value
Size of training data	70-90%	80%
Size of test data	10-30%	20%
Hidden layer number 1	1	1
Number of neurons	5, 10, 15, 20, 25, 30, 40, 50, 75, 100	25
Hidden layer transfer function	tansig, ReLU	tansig
Training algorithm	LM, BR	BR
Output layer transfer function	purelin	purelin
Iterations	1000	-
Objective goal	MSE 10^{-5}	-
Performance gradient (minimum)	10^{-5}	-

To ensure reproducibility, we evaluate the likelihood of consistent results. The ANN model was further validated by testing the chosen model configuration with five independent trials, where the model was trained and tested on different randomly selected data subsets using the 80:20 split. This is done because the initial values of optimization algorithms affect the final result in determining optimal weights and biases. Since these values are randomly selected, different results may be obtained in each run. The R^2 and RMSEs will be calculated to assess the reproducibility of the results. Across these repetitions, the network consistently achieved stable performance metrics, confirming that the predictive framework is both reliable and robust for forecasting CO_2 storage and oil production under varying data partitions. This systematic experimentation not only optimized the architecture but also ensured that the model maintained generalizability and computational efficiency in practical applications.

2.5 Statistical evaluation of ML models

The evaluation of the developed models consists of two key components: assessing the reproducibility of the results and evaluating the models using a comprehensive set of criteria, including MSE (mean squared error), RMSE (root mean square error), and R^2 (coefficient of determination). These evaluation processes are detailed below in Equations (2), (3), and (4).

$$MSE = \frac{1}{N}\sum_{i=1}^{N}\left[\!\left[(y)\right]\!\right]_{sim,\ i} - y_{pred,\ i}\Big)^2 \quad (2)$$

$$RMSE = \sqrt{\frac{1}{N}\sum_{i=1}^{N}\left[\!\left[(y)\right]\!\right]_{sim,\ i} - y_{pred,\ i}\Big)^2} \quad (3)$$

$$R^2 = 1 - \sum_{i=1}^{N}\frac{\left(y_{sim,\ i} - y_{pred,\ i}\right)^2}{\sum_{i=1}^{N}\left(y_{pred,\ i} - \bar{y}_{sim,\ i}\right)^2} \quad (4)$$

In this study, the Artificial Neural Network (ANN) toolbox in MATLAB 2024a was employed to develop the predictive model. The toolbox's built-in evaluation metrics—correlation coefficient (R) and mean square error (MSE)—served as the primary criteria for assessing model performance. To enhance interpretability, especially for non-technical audiences, the root mean square error (RMSE) was also included, as it presents the error in the same unit as the predicted output, making it more intuitive. Given that the study involves a regression task, where numerical predictions are made based on input-output relationships, scale-dependent evaluation metrics like MSE and RMSE were considered most appropriate. These metrics are well-suited for gauging the accuracy of regression-based machine learning models, ensuring meaningful performance evaluation.

3. Results and discussions

3.1 Reproducibility analysis

The reproducibility and robustness of the developed ANN models were evaluated by testing the optimal ANN configuration (25 hidden neurons, 80:20 split) in several separate trials. The findings showed consistent performance for both oil production and CO_2 storage, with minimal standard deviations in error metrics. This reproducibility bolsters confidence in the model's dependability by establishing that the network's predictive power is not unduly influenced by random initialization or particular data segmentation. Fig. 6 displays the calculated R^2 values used to evaluate the reliability of the created ANN models during the training and testing phases.

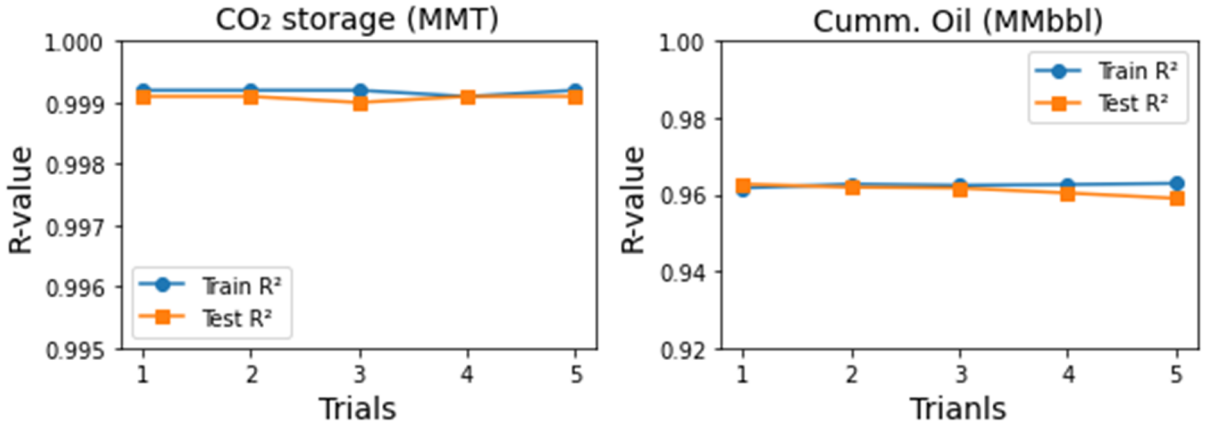

Fig. 6. Calculated R^2 values used to assess the reproducibility of the developed ANN models across the training and testing stages.

3.2 Performance of ML models

The fundamental mathematical equation that relates the input variables and the target variables (CO_2 storage and cumulative oil production) for the neural network can be written as shown in Equation (5):

$$Target\ (Unit) = f_{trFcn}\left\{b_n + \sum_{k=1}^{n}\left[W_k \times f_{trFcn}\left(b_{nk} + \sum_{i=1}^{m} W_{ik} X_i\right)\right]\right\} \quad (5)$$

$$h^1 = f^1(W^1 x + b^1) = tanh^{-1}(W^1 x + b^1) \quad (6)$$

$$y = f^2(W^2 h^1 + b^2) = purelin(W^2 h^1 + b^2) \quad (7)$$

where b_n = output layer bias, b_{nk} = hideen layer biases, W_k = output layer weights, W_{ik} = hidden layers weights, f_{trFcn} = transfer function, X_i = input features, and $Target$ = CO_2 storage or cumulative oil volume.

3.2.1 Explicit model equation for predicting CO_2 Storage

The ANN [9-25-1] structure, consisting of 9 input variables, 1 hidden layer with 25 neurons, was used to estimate CO_2 storage. The explicit derived neural network equation for the CO_2 storage capacity prediction can be written as shown in equation (8):

$$CO_2\ storage\ (tons) = f_{trFcn}\left\{b_n + \sum_{k=1}^{n}\left[W_k \times f_{trFcn}\left(b_{nk} + \sum_{i=1}^{m} W_{ik} X_i\right)\right]\right\} \quad (8)$$

This formulation demonstrates the ANN's multilayer processing, where the linear output layer makes sure that predictions are still interpretable on the physical scale of CO_2 storage (tons) and oil production (bbl). In contrast, the hidden layer's nonlinear transformation (tansig) captures the intricate, nonlinear relationships between reservoir/operational parameters and the targets. The predictive performance of the developed artificial neural network (ANN) demonstrates its ability to accurately map complex, high-dimensional, and nonlinear relationships between reservoir characteristics and CO_2 storage outcomes. The model achieves a high coefficient of determination ($R^2 = 0.998$) on the test dataset for CO_2 storage prediction, indicating exceptional generalization across diverse reservoir conditions. Importantly, the network's transparency allows for interpretability of the internal structure: the weights and biases can be analyzed to assess the relative influence of input variables on the predicted outcomes, offering insights into the governing reservoir and operational factors.

Fig. 7 provides a comprehensive evaluation of the ANN's performance. Fig. 7a presents the evolution of the mean squared error (MSE) throughout the training phase, showing smooth convergence and the absence of overfitting. Fig. 7b illustrates the residual error distribution, where errors are randomly scattered around zero, further confirming the model's robustness and lack of systematic bias. Fig. 7c displays the cross-plot of ground truth versus predicted CO_2 storage values for the test set. The data points closely align along the 1:1 line (Y = X), and the best-fit regression line exhibits a near-perfect overlap, underscoring the model's high predictive accuracy and reliability on unseen data. Table 3 details the optimized input weights, layer weights, and biases of the final trained ANN, representing the internal calibration that enables precise, non-linear mapping from input features to CO_2 storage predictions. Together, these metrics and visualizations confirm that the model not only delivers high accuracy but also maintains interpretability and generalization—key requirements for practical deployment in CCS-EOR reservoir analysis.

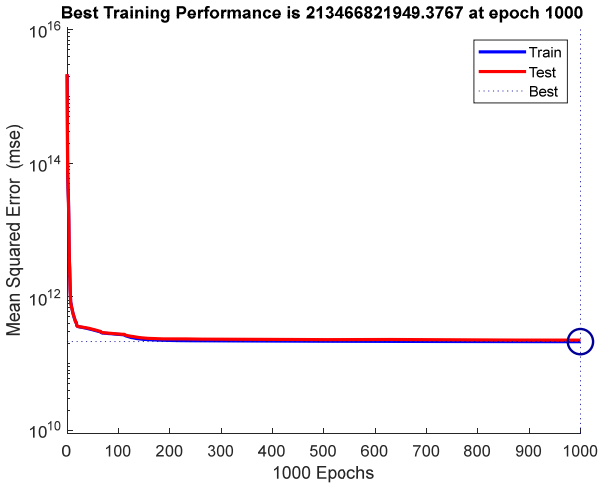

(a)

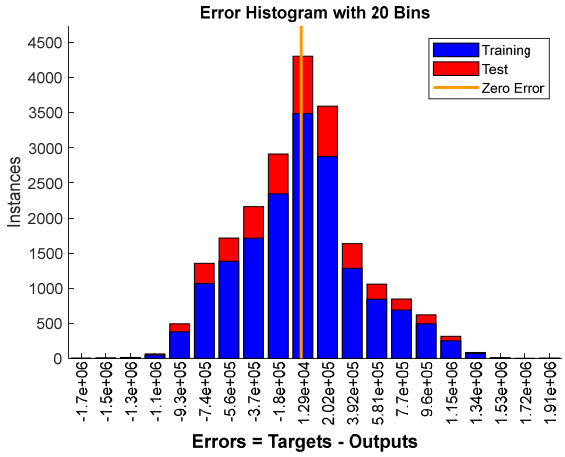

(b)

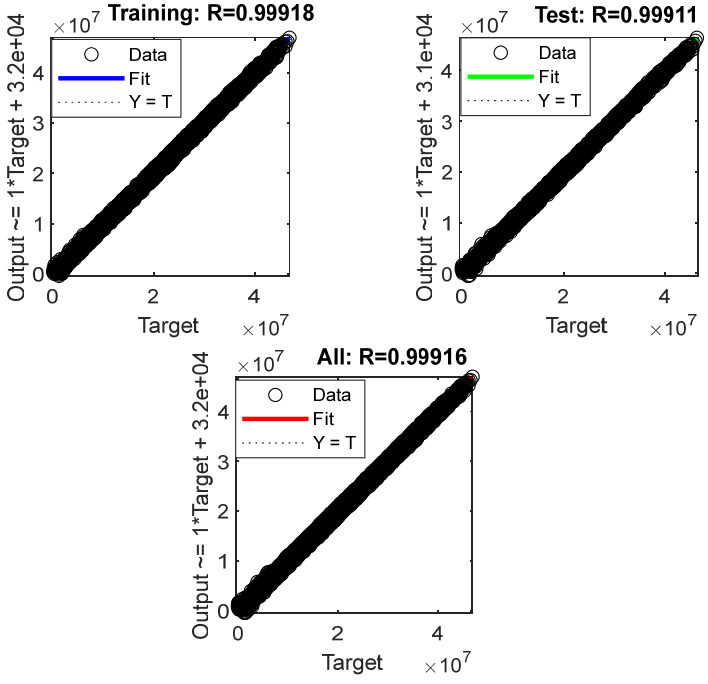

(c)

Fig. 7. Performance plot of ANN model for CO_2 storage prediction: (**a**) MSE minimization plot, (**b**) Residual plot, and (**c**) Prediction performance plots.

Tables 3. Weights and biases for the trained ANN model for CO_2 storage predictions.

IW											
X1	**X2**	**X3**	**X4**	**X5**	**X6**	**X7**	**X8**	**X9**	**b1**	**LW**	**b2**
-0.08846	-0.05568	0.756646	0.068209	1.116451	0.4074	0.005807	0.071812	-0.0467	1.547189	1.328371	2.106332137
-0.00198	-2.12785	0.035247	0.002891	0.030535	-0.02087	-0.00308	-0.00358	-0.01195	-2.74219	1.890766	
0.053546	-0.73113	-0.4511	-0.03194	-0.37202	-0.07714	-0.00681	-0.00095	0.017481	-0.84339	1.047468	
0.045092	-1.11237	-0.37914	-0.02711	-0.34234	-0.05903	-0.00576	0.00176	0.02242	-0.823	-0.53571	
0.13593	0.128101	-1.19845	-0.11002	0.058159	-0.55705	-0.01749	-0.08523	0.101879	-0.9585	-0.62696	
-0.33985	-0.28916	2.814848	0.247858	-0.23099	1.453861	0.003408	0.139988	-0.20701	3.551962	0.225515	
0.271595	0.19727	-2.73157	-0.21378	-1.26687	-1.00274	-0.00078	-0.18362	0.344445	-2.96006	-0.48604	
-0.37745	-0.14595	4.035872	0.329745	3.103106	0.766896	-0.00691	0.082909	-0.18338	4.9846	-1.00369	
-0.05862	-0.06617	0.521049	0.043168	0.314011	0.13969	0.002068	-0.041	0.018152	0.576871	-7.51789	
-0.01819	-0.00901	0.172881	0.013384	0.054672	-0.11207	-0.00045	0.022429	-0.01738	0.423097	6.997189	
-0.04514	-0.04506	0.413656	0.033631	0.275458	0.085488	0.003683	0.168216	0.019931	0.515815	-3.68297	
-0.03421	-0.0263	0.306815	0.023468	0.481008	0.218331	0.002069	0.026824	-0.02249	0.173274	3.410722	
0.097785	0.083777	-0.88121	-0.07124	-0.74752	-0.02356	-0.00611	-0.03769	0.052451	-0.12185	-1.24166	
0.006988	-2.64785	-0.01769	-0.00015	-0.01989	-0.03882	-0.00565	-0.00692	-0.01271	-2.80841	-0.86968	
0.261633	0.223917	-2.54234	-0.21748	-1.27076	-0.84699	0.000327	-0.23015	0.620857	-2.86405	0.320497	
-0.23701	-0.11674	2.461367	0.183357	1.893287	0.513089	0.000826	0.500008	-0.03884	2.891515	-0.83645	
-0.10252	-0.07602	0.939271	0.071053	0.435542	0.395373	-0.00374	-0.00973	-0.01553	0.655826	1.430245	
0.176746	0.386333	-1.39815	-0.12584	-1.61689	0.188754	-0.00663	-0.10373	0.083249	3.18604	0.181867	
-0.43255	-0.43977	4.455064	0.354593	3.524659	1.079384	-0.00461	0.186539	-0.18003	5.432624	1.322879	
-0.42361	-0.39566	4.27503	0.347054	3.340267	0.356279	0.013214	0.188704	-0.16996	5.199782	0.756144	
-0.25386	-0.14901	2.727084	0.204378	2.096303	0.56232	-0.00641	0.483918	-0.0744	2.94376	0.592915	
0.047136	0.041323	-0.41883	-0.03375	-0.25498	-0.09226	-0.00019	-0.02703	0.151126	-0.46616	4.436341	
-0.41396	-0.60002	4.124675	0.330477	3.230508	0.804982	0.006251	0.18042	-0.15147	5.029644	-1.22653	
0.056569	0.053492	-0.51382	-0.04306	-0.02707	-0.24563	-0.00275	-0.02764	0.036426	0.111427	-3.35098	
0.134406	0.086729	-1.17745	-0.09687	-0.98782	0.117538	-0.00818	-0.05673	0.054619	-1.37706	-1.04161	

The specific weights and biases of the trained artificial neural network (ANN) model created for CO_2 storage prediction are shown in Table 3. Nine input variables, one hidden layer with 25 neurons, and one output neuron made up the [9-25-1] structure used in the network architecture. Input-to-hidden weights (IW), hidden-layer biases (b1), hidden-to-output weights (LW), and the output bias (b2) are among the parameters that are presented.

To facilitate reproducibility and deployment, the complete weight matrices and bias vectors for both CO_2 storage and cumulative oil models are exported as JSON files (TrainedNN_FullCO2.json and TrainedNN_FullOil.json) and made available through the project's supplementary link. These JSON files contain the IW matrix [H x 9], LW matrix [1 x H], bias vectors b1 [H x 1] and b2 (scalar), per-feature normalization bounds (X_min, X_max), target normalization bounds, and the activation function specification, enabling any user to reproduce the forward pass without requiring the original training data. A representative subset of the weights is shown in Table 3 for reference.

3.2.2 Explicit model equation for predicting cumulative oil production

The ANN architecture [9–25–1] previously applied for CO_2 storage prediction was employed to model cumulative oil production. Using an 80:20 training-test split, this architecture balanced computational efficiency with predictive performance, avoiding overparameterization observed in deeper networks while outperforming simpler models. Fig. 8 shows the performance evaluation of the created ANN models for forecasting cumulative oil output and CO_2 storage capacity. Fig. 8a shows the mean squared error (MSE) during the training phase. Fig. 8b displays the residual error plot where the errors are dispersed randomly around zero. Also, the spread is broader for cumulative oil, which is in line with the higher unpredictability of production data. Finally, Fig. 8c presents the crossplot of ground truth and predicted values.

Due to the wider dynamic range inherent in cumulative oil volumes, prediction residuals exhibited greater variance relative to CO_2 storage; however, the measured versus predicted cross-validation plot (Fig. 8c) reveals strong correlation, with data points distributed closely around the identity line (Y = X). At elevated production volumes, a systematic negative bias emerges, with the regression slope deviating slightly below unity, indicative of underestimation of peak values. This heteroscedastic behavior aligns with the complex, nonlinear response characteristics typical of high-volume oil production. Despite this, model robustness is affirmed by stable root mean square error (RMSE) metrics across repeated cross-validation trials and a high coefficient of determination (R) ranging from 0.9617 to 0.9622.

Oil recovery dynamics exhibit greater stochasticity than CO_2 storage, arising from coupled effects of lithological heterogeneity, fluid-rock interactions, and reservoir pressure regimes. Nonetheless, the ANN effectively captures these nonlinear dependencies, as evidenced by the model's predictive fidelity. Table 4 details the optimized network weights and biases, while Equation (9) provides the explicit functional form, facilitating interpretability and reproducibility.

$$Cum.\,oil\ (bbl) = f_{trFcn}\left\{b_n + \sum_{k=1}^{n}\left[W_k \times f_{trFcn}\left(b_{nk} + \sum_{i=1}^{m} W_{ik}\,X_i\right)\right]\right\} \quad (9)$$

The trained ANN model weights and biases for predicting cumulative oil production are similarly exported in TrainedNN_FullOil.json and available through the supplementary file. A representative subset is shown in Table 4 for reference. The complete JSON files enable direct loading into the CCS-EOROptTool GUI application for instant inference without retraining.

Input-to-hidden weights (IW), hidden-layer biases (b1), hidden-to-output weights (LW), and output bias (b2) are among the values that are reported. By making these coefficients publicly available, the produced model is explicitly reproducible, enabling other practitioners and academics to immediately reconstruct and validate the ANN predictions without the need for retraining.

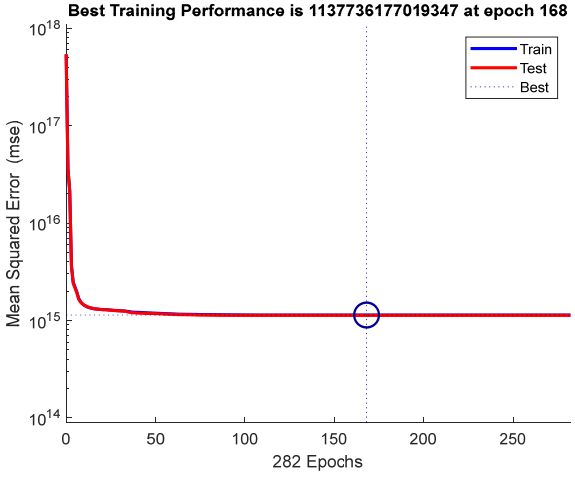

(a)

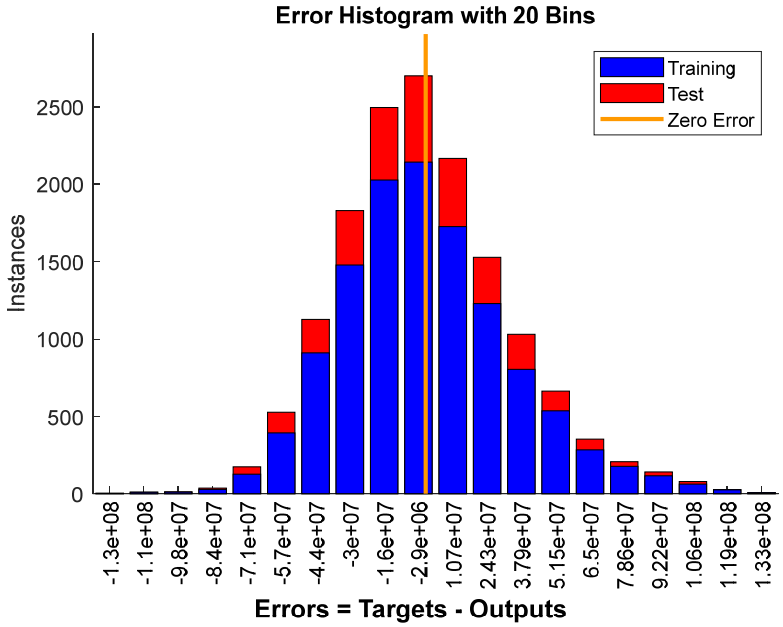

(b)

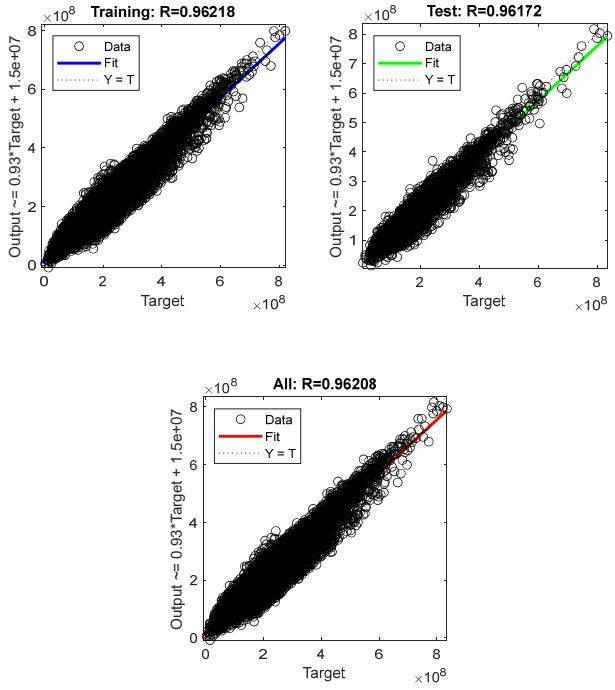

(c)

Fig. 8. Performance plot of ANN model for cumulative oil volume prediction: (**a**) MSE minimization plot, (**b**) Residual plot, and (**c**) Prediction performance plots.

Table 4. Weights and biases for the trained ANN model for cumulative oil production predictions.

IW											
X1	**X2**	**X3**	**X4**	**X5**	**X6**	**X7**	**X8**	**X9**	**b1**	**LW**	**b2**
0.62025	-0.02516	0.086321	0.462712	0.706271	0.059364	0.042639	0.016074	-0.03727	0.449305	0.469711	1.419301073
-0.31221	0.558425	0.406045	0.126607	0.335255	0.256476	0.719776	-0.17544	-0.00891	0.464376	-0.62773	
-0.30721	0.878283	0.692082	0.670215	0.613878	0.523635	0.035872	-0.2994	-0.01684	0.801249	-0.81851	
-0.38354	0.667566	0.478342	0.021718	0.312233	0.336174	-0.00346	-0.165	-0.02056	0.792286	2.612863	
0.225293	-0.34309	-0.23857	-0.1506	-0.14201	-0.90216	-0.02603	0.127959	0.009683	-0.47219	1.000622	
-0.16273	-0.5802	0.094475	0.031604	0.014875	0.019489	0.009576	-0.01169	-0.01736	-1.4154	-1.24038	
0.282018	-0.54389	-0.37493	-0.01784	-0.34492	-0.38998	0.713065	0.178164	0.014492	-0.50854	0.728236	
-1.05563	0.83881	0.605679	0.503592	0.418715	0.503118	-0.04072	-0.25381	0.03374	0.720136	-0.70845	
-0.40106	-0.16035	-0.11275	-0.49126	0.063944	-0.15401	0.059807	0.034168	0.015932	0.238631	1.165627	
-1.05868	0.86194	0.604818	-0.36867	0.655792	0.562054	0.011788	-0.24518	-0.01642	0.894809	-0.6072	
-0.60215	0.012809	0.032798	0.798418	0.56308	-0.02727	-0.00781	-0.02101	-0.03143	-0.22222	-0.36331	
0.44085	0.316925	0.170751	0.577037	0.928807	0.176766	0.024739	-0.04153	-0.0076	-1.47783	0.84637	
-0.14003	-0.34007	-0.27176	0.430957	-0.56214	-0.30398	-0.06168	0.098389	0.021775	-0.03178	1.403792	
-0.29264	0.535181	0.489006	-0.0526	0.423347	-0.32687	-0.05835	-0.15377	0.005623	0.289933	-0.8841	
0.041706	1.126247	-0.06696	0.044348	-0.11994	-0.2739	-0.01343	0.01862	0.014195	0.702144	-0.34581	
0.457236	-0.8432	-0.65444	0.05916	0.077964	-0.48334	-0.02011	0.260779	0.010115	-0.66172	0.978059	
0.013865	0.296271	0.243471	-1.00019	-0.54412	0.325597	-0.01346	-0.16171	0.006768	-0.39412	-0.15837	
0.544179	0.491061	0.252148	-0.725	-0.04859	0.359355	0.027597	-0.10223	0.019123	-1.50435	0.75002	
-0.53856	0.122118	0.02297	0.806572	-0.44031	-0.10596	-0.11555	-0.05892	-0.00314	-0.36824	-0.51612	
-0.07506	0.778079	0.543195	-0.32404	0.626069	0.491833	0.031575	-0.21296	-0.03572	-0.31859	0.933853	
0.550168	-0.77314	-0.58914	-0.2155	-0.36301	-0.50254	0.002386	0.270244	-0.0015	-0.47774	-2.43531	
-0.26957	0.101584	0.143808	0.518925	-0.08732	0.699909	-0.13647	-0.15436	-0.01719	0.760482	0.587291	
-0.50306	0.666851	0.683476	-0.05349	0.518002	-0.21636	0.021651	-0.1791	0.031033	-0.01526	0.375174	
0.961665	-0.33342	-0.20575	0.688637	-0.44952	-0.09255	-0.07392	0.097011	-0.00203	1.803846	-0.88854	
-0.27314	0.260476	0.185342	0.501498	-0.09167	0.248052	-0.07898	-0.10633	-0.0107	-0.80912	2.036249	

In Table 5, the prediction performance of the ANN models was evaluated across the training and test subsets for CO_2 storage and cumulative oil production data. Among the predictions, the CO_2 storage prediction shows the best overall performance, achieving the highest R^2 values and the lowest RMSE in comparison with the cumulative oil production. Although CO_2 storage prediction demonstrated better performance, there is consistency across the training and testing phases. This result highlights the reproducibility and generalization of the ANN models for predicting CO_2 storage and cumulative oil production.

Table 5. Summary of statistical error metrics for evaluating the performance of the model.

	Samples	Phases	Error metric	
			R^2	RMSE (10^6)
CO_2 Storage	16, 954	Training	0.9984	0.4629
	4,239	Test	0.9982	0.4785
Cum. Oil	12,100	Training	0.9258	33.3226
	3,026	Test	0.9247	34.2476

3.3 Sensitivity assessment via relevancy factor

Determining how each input contributes to the goals is crucial to comprehending how geology and operational controls influence the forecasts. The relevancy factor (RF) was used to quantify feature influence (Longe et al., 2020). The inverse tendency is indicated by RF < 0, while RF > 0 implies that increasing an input tends to raise the anticipated target. The magnitudes of each predictor are comparable across variables because they were all scaled from min to max. These impacts are summed up in the RF profile in Figs 9 and 10 for both CO_2 storage and cumulative oil.

The connection-weights algorithm (Olden, 2004; Olden and Jackson, 2002) is used to quantify the relative influence of each input variable. For a feed-forward network with i = 1,...,N inputs, j = 1,...,H hidden neurons, and a single output, let IW_{ij} denote the weight from input i to hidden neuron j, and let LW_j denote the weight from hidden neuron j to the output. The raw connection-weights contribution of input i is defined as

$$CW_i = \sum_{j=1}^{H} (IW_{ij} \times LW_j) \quad (10)$$

Because all inputs were min-max normalised to [0, 1] before training, CW_i values are directly comparable across variables in both magnitude and sign. The relevancy factor (RF) reported in Figs. 9 and 10 are the signed, normalised version:

$$RF_i = \frac{CW_i}{\sum_{k=1}^{N} |CW_k|} \quad (11)$$

so that $\sum_{i=1}^{N} |RF_i| = 1$, the sign indicates whether increasing input i increases ($RF_i > 0$) or decreases ($RF_i < 0$) the predicted target, and the magnitude expresses the share of total signed influence. The connection-weights method was chosen over Garson's algorithm because Olden et al. (Olden, 2004) demonstrated in a Monte Carlo benchmark that it most accurately recovers known true variable importances while preserving sign information.

Based on Figs. 9 and 10, it can be inferred that thickness, permeability, porosity, and injection rate exhibit positive correlations with CO_2 storage and cumulative oil volume. This outcome is evident from the bars pointing towards the positive axes, indicating that an increase in these parameters increases CO_2 storage and cumulative oil volume in ROZs. Conversely, bottom hole pressure, depth, and S_{orw} exhibit negative correlations with CO_2 storage and cumulative oil volume, suggesting that an increase in these two parameters leads to a decrease in CO_2 storage. Consequently, the following explanations can be provided for each parameter:

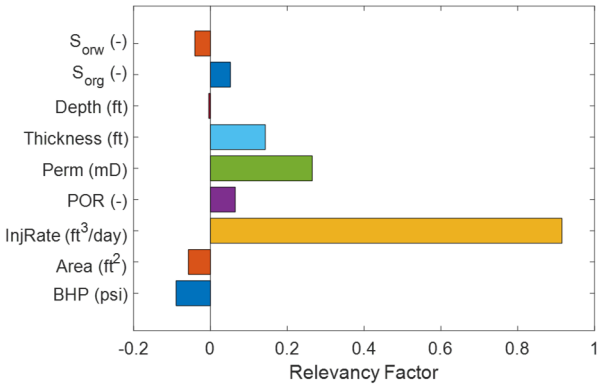

Fig. 9. Summary plot of feature importance depicting the influence of each input feature on CO_2 storage with the relevancy factor in the ANN model.

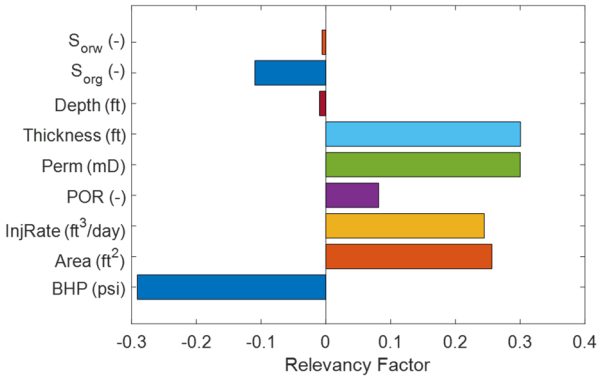

Fig. 10. Summary plot of feature importance depicting the influence of each input feature on cumulative oil production with the relevancy factor in the ANN model.

Injection rate (ft^3/day): For both the CO_2 storage and the cumulative oil, the injection rate has strong positive RF. Higher injection rates enhance injectivity, expand the pressure-support region, and boost sweep efficiency, all of which raise the injected CO_2 mass and maintain oil displacement. For CO_2 storage and CO_2-EOR systems, rate/injectivity management is a key operational parameter, which is consistent with previous evaluations (Chen and Pawar, 2018, 2019a, 2019b; Davoodi et al., 2024a).

Permeability (mD): shows a substantial positive RF, which is slightly stronger for cumulative oil. Increased permeability results in a more favorable mobility

environment, which raises injectivity, sweep efficiency, and displacement ratio. It also increases transmissibility and decreases viscous losses. Wider storage reviews come to the same conclusion about flow-capacity controls (Ali et al., 2022), and new reservoir-condition CO_2–brine relative-permeability datasets and associated analyses report mobility/endpoint behavior consistent with this sensitivity (Mascle et al., 2025; Reisi et al., 2023).

Formation thickness (ft): Thickness is frequently the most important geologic variable for oil and exhibits a strong positive RF for both outputs. In line with recent syntheses that project rock volume $(A.h.\phi)$ and kh as a precursor parameter on capacity and performance, increasing the thickness of the formation expands the pore volume and fracture conductivity (kh), thereby increasing contact volume and drainage pathways (Bashir et al., 2024).

Areal extent (ft^2): The areal extent has a positive RF for oil production targets: a greater area boosts the reservoir volume in contact over time and improves areal sweep, which is in line with pattern-scale evaluations in current storage and EOR studies (Chen and Pawar, 2018, 2019a, 2019b; Davoodi et al., 2024a). Conversely, the ANN model indicates a negative for the RF reservoir areal extent with respect to CO_2 storage. This trend does not imply that larger reservoirs possess lower intrinsic storage capacity. Instead, it reflects the combined effects of fixed grid resolution, constant well configuration, and operational injection constraints used in the simulations. As the areal extent increases without proportional refinement of grid discretization or scaling of injection strategy, sweep efficiency and numerically resolved trapping mechanisms decrease, resulting in lower injected and retained CO_2 within the simulated timeframe. Thus, the observed trend represents a reduction in storage efficiency rather than a violation of volumetric storage principles.

Porosity (ϕ): Porosity exhibits a moderately positive RF. As the area and thickness of the formation define the rock volume, the incremental contribution of porosity decreases, which is consistent with storage-capacity syntheses that treat PV as a baseline constraint (Ali et al., 2022; Bashir et al., 2024). Higher porosity increases pore volume, which raises CO_2 capacity and OOIP.

Residual saturations (S_{org}, S_{orw}): The ANN model indicates a negative relevancy factor of residual water saturation (S_{orw}) with cumulative oil production. While ROZ development typically initiates at Sorw and, under idealized conditions, a higher Sorw may imply greater initial oil-in-place, the predicted trend reflects the dynamic impact of Sorw on CO_2 displacement efficiency rather than static oil volume. Higher Sorw reduces relative permeability to oil and CO_2, increases capillary trapping, and limits CO_2 sweep efficiency, leading to lower incremental oil recovery during injection. This behavior is consistent with consistent with ROZ physics and pore-scale observations of residual and capillary trapping and hysteresis effects in CO_2–brine–oil systems, where increased irreducible water saturation constrains phase mobility and effective displacement despite higher initial oil saturation (Chen and Pawar, 2018, 2019a, 2019b; Iglauer et al., 2019; Sedaghatinasab et al., 2021).

Bottom-hole flowing pressure (psi): Bottomhole pressure strongly influences CO_2-EOR performance. Under conditions approaching CO_2-oil miscibility, higher BHP increases oil recovery by improving miscible displacement and reducing interfacial tension. In immiscible scenarios, BHP primarily affects CO_2 density and sweep efficiency. The ANN-derived relevancy factor for BHP reflects its combined effect on pressure-driven miscibility and displacement efficiency, emphasizing the importance of injection pressure optimization in ROZ CO_2-EOR (Chen and Pawar, 2018, 2019a, 2019b; Davoodi et al., 2024a).

Depth (ft): Depth adds very little extra predictive information within our sampled depth range because it has near-zero RF for both CO_2 storage and cumulative oil. Additionally, rock volume $(A.h.\phi)$ and flow capacity (kh) are two other informative variables, which either already capture or have a moderate impact on depth-related pressure–temperature effects. Recent CCS syntheses that put injectivity and reservoir characteristics ahead of "depth alone" (Bashir et al., 2024; Massarweh and Abushaikha, 2024) are consistent with these findings.

3.4 Comparison with other published studies

Table 6 presents a comparison between the ANN model developed in this study and several high-performing alternatives from literature. When compared to previously published models, including standalone and hybrid LSSVM variants as well as a committee-learning CML-GPR ensemble, the proposed ANN slightly outperforms CML-GPR in predicting CO_2 storage. It significantly outperforms both standalone and optimized LSSVM models in terms of test RMSE, while matching their R^2. For cumulative oil prediction, advanced LSSVM-GWO models retain the lead, with the ANN trailing. The published LSSVM-GWO models of Davoodi et al. (Davoodi et al., 2025d) achieve a higher cumulative-oil R^2 (≈0.99) on the same dataset. This gap arises from four identifiable, non-mutually exclusive sources, none of which reflects underfitting of the present model. (i) Difference in datapoints, (ii) Functional capacity. LSSVM with a Gaussian kernel projects the nine input features into a Reproducing Kernel Hilbert Space whose effective dimension equals the number of training samples (here ≈ 12,000), providing a far higher capacity for fitting non-smooth response surfaces than a single hidden layer of 25 tansig units (Suykens and Vandewalle, 1999). For a target like cumulative oil that spans more than six orders of magnitude and is governed by a near-bilinear interaction between BHP, injection rate, and Sorw, that additional capacity translates into a small but consistent reduction in residual error. (iii) Hyperparameter optimization: Grey Wolf Optimization tunes the LSSVM regularization γ and kernel width σ against the test loss directly, which is known to extract the last ≈ 1–2% of R^2 in regression tasks but at the cost of optimism bias when the test set is reused as a validation set during the metaheuristic loop (Cawley and Talbot, 2010). (iv) Interpretability–accuracy trade-off. Our explicit objective (Section 1.3) was a model that can be written down in closed form, redeployed by any reader from a one-page weight table, and inspected by the connection-weights algorithm. Kernel models cannot satisfy this objective without storing the full set of support vectors

and α coefficients. The 0.925 vs 0.99 difference in R^2 (a residual that on test samples corresponds to an RMSE of 3.42×10^7 bbl out of an output range of 8.35×10^8 bbl, i.e., ≈ 4%) is therefore the deliberate price paid for explicit, deployable, and interpretable structure. Train–test gaps for both ANN targets remain below 0.001 in R^2 (Table 5), confirming that the gap to LSSVM-GWO does not arise from overfitting of the present model.

Table 6. Comparison of the ANN model and published studies. The assessment of CO_2 storage and cumulative oil production is based on performance on the test dataset.

Target	Reference	No. of dataset	Best model	Subset	Metrics	
					R^2	RMSE (10^6)
CO_2 storage	Davoodi et al., 2024b	10295	LSSVM	Train	0.9987	0.4052
				Test	0.997	0.6224
	Davoodi et al., 2025c	32425	LSSVM-GWO	Train	0.9984	0.4478
				Test	0.9954	0.7811
	Davoodi et al., 2025d	21193	CML-GPR	Train	0.9989	0.3692
				Test	0.9982	0.4883
	This study	21193	AN N	Train	0.9984	0.4629
				Test	0.9982	0.4785
Cum. oil	Davoodi et al., 2024b	10295	LSSVM	Train	0.9952	9.7392
				Test	0.992	12.5143
	Davoodi et al., 2025c	32425	LSSVM-GWO	Train	0.9976	6.6677
				Test	0.995	10.1245
	Davoodi et al., 2025d	21193	CML-GPR	Train	0.9941	10.4237
				Test	0.9897	13.6834
	This study	15126	ANN	Train	0.9258	33.3226
				Test	0.9247	34.2476

3.5 Software implementation and model deployment

The development of a machine learning model is only valuable when its predictions can be reliably accessed and applied in real-world scenarios. As such, deployment is a critical step equally important as model development in translating machine learning outputs into operational decision-making tools. In this study, the trained artificial neural network (ANN) models were deployed via a standalone software application designed for field use in ROZs. To ensure accessibility, portability, and operational reliability, the ANN models were embedded in a lightweight graphical user interface (GUI) application named CCS-EOROptTool, built using Python and the PyQt5 framework. The application runs offline on standard Windows systems without requiring internet access, thereby supporting fast and secure inference in remote or bandwidth-limited field settings. A desktop-based solution was deliberately chosen over web or mobile alternatives to minimize data handling risk and latency, while also maximizing user autonomy.

The GUI is structured around intuitive, field-relevant controls that accept nine key reservoir and operational input parameters. It then loads the trained model weights exported from MATLAB in JSON format and instantly returns two actionable outputs: predicted CO_2 storage mass (tonnes) and cumulative oil production (barrels). The separation of a thin presentation layer from a compact inference layer ensures computational efficiency and modular maintainability. The GUI responds in under one second, making it suitable for rapid scenario analysis and real-time decision support. An overview of the deployed application and its typical user workflow is presented in the following Fig. 11. To promote reproducibility and facilitate further development, the full implementation code for CCS-EOROptTool is made publicly available through a dedicated GitHub repository (CCS_EOROptTool). This ensures transparent access to the model and its deployment architecture.

3.6 Uncertainty propagation module

The deterministic forward pass of the trained [9–25–1] ANN is computationally inexpensive (sub-millisecond per evaluation on a standard CPU because it consists of one matrix–vector multiplication, a tansig activation, and a linear output mapping). This allows tens of thousands of evaluations to be executed in seconds, making sampling-based uncertainty propagation a natural fit. In this version of CCS-EOROptTool, the user can optionally specify, for each of the nine input variables, either (a) a coefficient of variation (CV) representing measurement/characterization uncertainty around a deterministic best-estimate value, or (b) explicit lower/upper bounds. The tool then draws N = 10,000 Latin Hypercube samples (LHS) from independent truncated-normal or uniform marginals (consistent with the LHS strategy used to construct the training dataset; see Section 3.1), evaluates the ANN at each sample, and reports for both targets (CO_2 storage mass and cumulative oil): the mean, standard deviation, P10/P50/P90 percentiles, and the empirical 95% confidence interval. A tornado plot of the variance contribution by the input variable is also rendered. LHS was chosen over crude MC because it provides lower-variance estimates of the output mean and percentiles for the same sample size, which is the standard practice for proxy-model UQ in subsurface applications (Helton and Davis, 2003; Mishra et al., 2018; Vo Thanh et al., 2020b). This module directly addresses the need for probabilistic assessment in CO_2 storage and EOR problems, where characterization uncertainty in parameters such as permeability, porosity, and BHP can significantly influence predicted storage capacity and oil recovery.

(**a**)

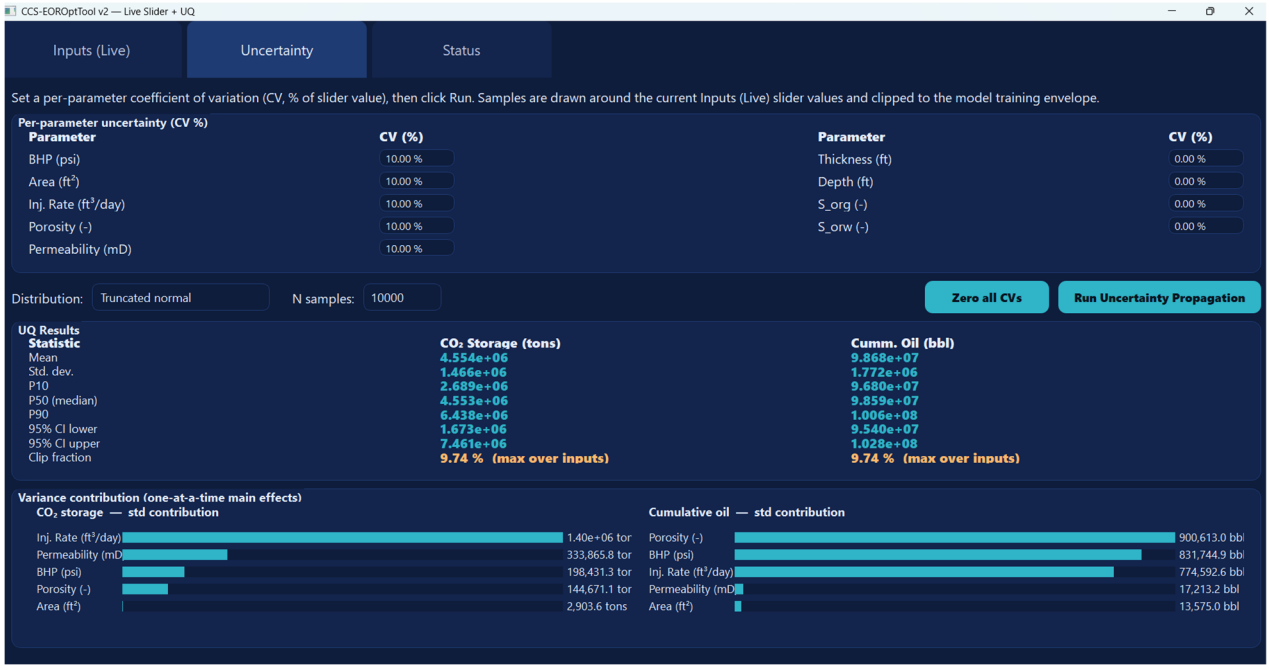

(**b**)

Fig. 11. Graphical user interface of the CCS-EOROptTool desktop application. (**a**) Deterministic prediction interface: nine reservoir and operational input parameters are controlled via interactive sliders with coupled spin-box entry. Predictions of CO_2 storage mass (tons) and cumulative oil production (bbl) update in real time as any slider is adjusted, enabling rapid exploration of the response surface without switching views. (**b**) Monte Carlo uncertainty propagation interface: users specify a per-parameter coefficient of variation (CV, % of the slider value) representing measurement or characterization uncertainty. Upon execution, 10,000 Latin Hypercube samples are drawn from truncated-normal marginals, propagated through the trained ANN in a single vectorized forward pass, and summarized as mean, standard deviation, P10/P50/P90 percentiles, and the 95% empirical confidence interval for both CO_2 storage and cumulative oil production. A pair of tornado plots display the one-at-a-time variance contribution of each uncertain input, identifying which parameters dominate the output spread and therefore warrant prioritized characterization. In the example shown, a 10% CV is applied to BHP, area, injection rate, porosity, and permeability; the tornado plots reveal that injection rate and porosity are the dominant contributors to CO_2 storage and oil production uncertainty, respectively.

3.7 Domain of applicability and transfer to other settings

The trained ANN model is statistically valid only inside the nine-dimensional hyperbox defined by the input ranges in Table 1. Within this envelope, a leave-one-region-out (LORO) cross-validation experiment, in which the dataset is partitioned by LHS region, and the model is retrained on seven octants and tested on the held-out octant, yields a mean test R^2 of approximately 0.987 for CO_2 storage and 0.943 for cumulative oil, confirming robust interpolation. However, the underlying simulation deck is based on a Goldsmith-Landreth-type carbonate (high-permeability, dolomitic, weakly fractured), so the trained model implicitly inherits the relative-permeability hysteresis curves, capillary pressure curves, MMP, and PVT package representative of San Andres carbonates. Applicability to (i) siliciclastic ROZs (e.g., Tensleep, Morrow), (ii) low-permeability fractured carbonates, or (iii) ROZs with significantly different brine salinity or oil API would require either re-training on a representative simulation suite or a transfer-learning step. The CCS-EOROptTool GUI enforces this boundary by refusing to make predictions when any input lies outside the training envelope and issuing a warning to the user. Direct application of the current weights and biases outside this envelope is not recommended (Honarpour et al., 2010; Koperna et al., 2006; Trentham et al., 2015).

4. Conclusions

This study presents a transparent and interpretable data-driven framework for predicting CO_2 storage capacity and cumulative oil production in residual oil zones using an artificial neural network trained on more than 21,000 compositional reservoir simulations. The framework advances prior work in four main ways: it provides the model in explicit closed form, enables mechanistic interpretation through signed variable relevance, validates architectural robustness through systematic hyperparameter optimization, and delivers a lightweight deployable tool with built-in uncertainty quantification. Together, these features make the model reproducible, explainable, and directly usable for practical reservoir screening and decision support.

The results show that a properly calibrated shallow neural network can achieve strong predictive performance on structured reservoir data while remaining simpler and more interpretable than more complex alternatives. By embedding the model in the CCS-EOROptTool interface and extending it with Monte Carlo uncertainty analysis, the study moves beyond proof-of-concept prediction toward a practical workflow for rapid, risk-informed screening of ROZ candidates.

The model remains valid only within the nine-parameter training envelope and currently reflects the fluid and rock properties of Permian Basin dolomitic carbonates. Broader applicability will require retraining or transfer learning with datasets spanning additional lithologies, basin conditions, and operational strategies. Future work should therefore focus on expanding the simulation base, incorporating dynamic injection schemes, and integrating field data for calibration and validation. Overall, by combining explicit formulation, physical interpretability, robustness testing, and deployable uncertainty-aware prediction, this study provides a screening-stage proxy for the high-fidelity simulator, not as a replacement for history-matched field models.

Supplementary Materials

The supplementary file and code for CCS-EOROptTool have been made available on the GitHub page: https://github.com/Keshi-23/CCS_EOROptTool.git.

Author Contributions

Conceptualization, P.L. and Z.I.; methodology, P.L. and O.E.; software, P.L., Z.I. and O..; formal analysis, P.L., J.O. and O.E.; writing—original draft preparation, S.L.; writing—review and editing, P.L., S.D., O.E., and J.O.; visualization, P.L. J.O., and O.E.; supervision, S.D. and P.L. All authors have read and agreed to the published version of the manuscript

Funding

This research received no external funding.

Conflict of interest

The authors declare no conflict of interest.

Use of AI and AI-assisted Technologies

During the preparation of this work, the authors used the tools Grammarly, Inc. Claude and ChatGPT for language validation and refinement. After using those tools, the authors reviewed and edited the content as needed and take full responsibility for the content of the publication.

Nomenclature

ANN	Artificial neural network
A	Area
b1	Biases for hidden layer neurons in ANN
b2	Bias for the output neuron in ANN
BHP	Bottom-hole pressure (psi)
BR	Bayesian regularization
CCS	Carbon capture and storage
CCS-EOR	Carbon capture, storage, and enhanced oil recovery
CMG-GEM	Compositional reservoir simulator (Computer Modelling Group)
CO_2	Carbon dioxide
Cum. Oil	Cumulative oil production (bbl)
EOR	Enhanced oil recovery
GUI	Graphical User Interface (CCS-EOROptTool)
INJRATE	CO_2 injection rate (ft^3/day)

IW	Input-to-hidden weights in ANN
Kr	Relative permeability
LHS	Latin Hypercube Sampling
LM	Levenberg-Marquardt
LW	Hidden-to-output weights in ANN
MMP	Minimum Miscibility Pressure (psi)
MSE	Mean squared error
Pc	Capillary pressure
PERM	Permeability (mD)
purelin	Linear activation function
RMD	Robust Mahalanobis Distance
RMSE	RMSE–Root mean squared error
ROZs	Residual oil zones
R^2	Coefficient of determination
Sorg	Oil saturation at residual gas
Sorw	Oil saturation at residual water

References

Abbaszadeh, M., Shariatipour, S. M. Investigating the Impact of Reservoir Properties and Injection Parameters on Carbon Dioxide Dissolution in Saline Aquifers. Fluids, 2018, 3(4): 76.

Agwu, O. E., Alatefi, S., Alkouh, A., Abdel Azim, R., Wee, S. C. Carbon capture using ionic liquids: An explicit data driven model for carbon (IV) Oxide solubility estimation. Journal of Cleaner Production, 2024, 472: 143508.

Ahmadi, M. A., Zendehboudi, S., James, L. A. Developing a robust proxy model of CO_2 injection: Coupling Box–Behnken design and a connectionist method. Fuel, 2018, 215: 904–914.

Ahmed, U., Meehan, D. N. Unconventional oil and gas resources: exploitation and development. CRC Press, 2016.

Ajayi, T., Gomes, J. S., Bera, A. A review of CO2 storage in geological formations emphasizing modeling, monitoring and capacity estimation approaches. Petroleum Science, 2019, 16: 1028–1063.

Al Eidan, A. A., Bachu, S., Melzer, L. S., Lars, E. I., Ackiewicz, M. Technical Challenges in the Conversion of CO2-EOR Projects to CO2 Storage Projects, in: SPE Asia Pacific Enhanced Oil Recovery Conference. Presented at the SPE Asia Pacific Enhanced Oil Recovery Conference, SPE, Kuala Lumpur, Malaysia, 2015.

Ali, M., Jha, N. K., Pal, N., Keshavarz, A., Hoteit, H., Sarmadivaleh, M. Recent advances in carbon dioxide geological storage, experimental procedures, influencing parameters, and future outlook. Earth-Science Reviews, 2022, 225: 103895.

Al-Khdheeawi, E. A., Vialle, S., Barifcani, A., Sarmadivaleh, M., Iglauer, S. Influence of injection well configuration and rock wettability on CO_2 plume behaviour and CO_2 trapping capacity in heterogeneous reservoirs. Journal of Natural Gas Science and Engineering, 2017, 43: 190–206.

Al-Mudhafar, W. J. Polynomial and nonparametric regressions for efficient predictive proxy metamodeling: Application through the CO2-EOR in shale oil reservoirs. Journal of Natural Gas Science and Engineering, 2019, 72: 103038.

Al-Mudhafar, W. J., Rao, D. N., Srinivasan, S. Geological and production uncertainty assessments of the cyclic $$\text{CO}_2$$ CO 2 -assisted gravity drainage EOR process: a case study from South Rumaila oil field. Journal of Petroleum Exploration and Production Technology, 2019, 9: 1457–1474.

Al-Mudhafar, W. J., Rao, D. N., Srinivasan, S., Vo Thanh, H., Al Lawe, E. M. Rapid evaluation and optimization of carbon dioxide-enhanced oil recovery using reduced-physics proxy models. Energy Science & Engineering, 2022, 10: 4112–4135.

Al-Shargabi, M., Davoodi, S., Wood, D. A., Rukavishnikov, V. S., Minaev, K. M. Carbon Dioxide Applications for Enhanced Oil Recovery Assisted by Nanoparticles: Recent Developments. ACS Omega, 2022, 7: 9984–9994.

Alves, D. T. S., Lima, G. B. A. Establishing an onshore pipeline incident database to support operational risk management in Brazil - Part 2: Bowtie proposition and statistics of failure. Process Safety and Environmental Protection, 2021, 155: 80–97.

Ampomah, W., Balch, R., Cather, M., Will, R., Gunda, D., Dai, Z., Soltanian, M. Optimum design of CO2 storage and oil recovery under geological uncertainty. Applied energy, 2017, 195: 80–92.

Bahrami, P., James, L. A. Screening of waterflooding using smart proxy model coupled with deep convolutional neural network. Geoenergy Science and Engineering, 2023, 221: 111300.

Balch, R., McPherson, B. Integrating Enhanced Oil Recovery and Carbon Capture and Storage Projects: A Case Study at Farnsworth Field, Texas, in: SPE Western Regional Meeting. Presented at the SPE Western Regional Meeting, SPE, Anchorage, Alaska, USA, 2016.

Bashir, A., Ali, M., Patil, S., Aljawad, M. S., Mahmoud, M., Al-Shehri, D., Hoteit, H., Kamal, M. S. Comprehensive review of CO2 geological storage: Exploring principles, mechanisms, and prospects. Earth-Science Reviews, 2024, 249: 104672.

Braspenning, P. J. Artificial neural networks: an introduction to ANN theory and practice. Springer Science & Business Media, 1995.

Burden, F., Winkler, D. Bayesian regularization of neural networks. Artificial neural networks: methods and applications, 2008, 23–42.

Cawley, G. C., Talbot, N. L. C. On Over-fitting in Model Selection and Subsequent Selection Bias in Performance Evaluation. Journal of Machine Learning Research, 2010, 11: 2079–2107.

Chen, B., Pawar, R. Capacity Assessment of CO2 Storage and Enhanced Oil Recovery in Residual Oil Zones, in: SPE Annual Technical Conference and Exhibition. Presented at the SPE Annual Technical Conference and Exhibition, SPE, Dallas, Texas, USA, 2018.

Chen, B., Pawar, R. J. Characterization of CO2 storage and enhanced oil recovery in residual oil zones. Energy, 2019a, 183: 291–304.

Chen, B., Pawar, R. J. Capacity assessment and co-optimization of CO2 storage and enhanced oil recovery in residual oil zones. Journal of Petroleum Science and Engineering, 2019b, 182: 106342.

Chen, S., Li, H., Yang, D., Tontiwachwuthikul, P. Optimal Parametric Design for Water-Alternating-Gas (WAG) Process in a CO2-Miscible Flooding Reservoir. Journal of Canadian Petroleum Technology, 2010, 49: 75–82.

Dai, Z., Middleton, R., Viswanathan, H., Fessenden-Rahn, J., Bauman, J., Pawar, R., Lee, S. -Y., McPherson, B. An integrated framework for optimizing CO2 sequestration and enhanced oil recovery. Environmental Science & Technology Letters, 2014a, 1: 49–54.

Dai, Z., Stauffer, P. H., Carey, J. W., Middleton, R. S., Lu, Z., Jacobs, J. F., Hnottavange-Telleen, K., Spangler, L. H. Pre-site Characterization Risk Analysis for Commercial-Scale Carbon Sequestration. Environmental Science & Technology, 2014b, 48: 3908–3915.

Dai, Z., Xu, L., Xiao, T., McPherson, B., Zhang, X., Zheng, L., Dong, S., Yang, Z., Soltanian, M. R., Yang, C., et al. Reactive chemical transport simulations of geologic carbon sequestration: Methods and applications. Earth-Science Reviews, 2020, 208: 103265.

Davoodi, S., Al-Shargabi, M., Wood, D. A., Mehrad, M., Rukavishnikov, V. S. Carbon dioxide sequestration through enhanced oil recovery: A review of storage mechanisms and technological applications. Fuel, 2024a, 366: 131313.

Davoodi, S., Longe, P.O., Makarov, N., Wood, D. A., Vo Thanh, H., Mehrad, M. Advanced Optimized Deep-Learning Model for Precise Evaluation of Subsurface Carbon Dioxide Trapping Efficiency. Energy Fuels, 2025a, 39: 3966–3992.

Davoodi, S., Longe, P. O., Thanh, H. V., Mehrad, M., Mohammadi, A. H., Burnaev, E. Machine-learning models for predicting CO2 solubility in various brine systems: implications for carbon geo-storage. Journal of Molecular Liquids, 2025b, 435: 128122.

Davoodi, S., Thanh, H. V., Wood, D. A., Mehrad, M., Al-Shargabi, M., Rukavishnikov, V. S. Machine learning insights to CO2-EOR and storage simulations through a five-spot pattern–a theoretical study. Expert Systems with Applications, 2024b, 250: 123944.

Davoodi, S., Thanh, H. V., Wood, D. A., Mehrad, M., Muravyov, S. V., Rukavishnikov, V. S. Carbon dioxide storage and cumulative oil production predictions in unconventional reservoirs applying optimized machine-learning models. Petroleum Science, 2025c, 22: 296–323.

Davoodi, S., Vo Thanh, H., Wood, D. A., Mehrad, M., Al-Shargabi, M., Rukavishnikov, V. S. Machine learning insights to CO2-EOR and storage simulations through a five-spot pattern – a theoretical study. Expert Systems with Applications, 2024c, 250: 123944.

Davoodi, S., Vo Thanh, H., Wood, D. A., Mehrad, M., Al-Shargabid, M., Rukavishnikov, V. S. Committee machine learning: A breakthrough in the precise prediction of CO2 storage mass and oil production volumes in unconventional reservoirs. Geoenergy Science and Engineering, 2025d, 245: 213533.

Ejehu, O., Moghanloo, R., Nashed, S. Predictive Modeling and Simulation of CO2 Trapping Mechanisms: Insights into Efficiency and Long-Term Sequestration Strategies. Energies, 2025, 18: 4071.

Ettehadtavakkol, A., Lake, L. W., Bryant, S. L. CO2-EOR and storage design optimization. International Journal of Greenhouse Gas Control, 2014, 25: 79–92.

Foresee, F. D., Hagan, M. T. Gauss-Newton approximation to Bayesian learning. Presented at the Proceedings of international conference on neural networks (ICNN'97), IEEE, 1997.

Gibson-Poole, C. M., Svendsen, L., Underschultz, J., Watson, M. N., Ennis-King, J., Ruth, P. J. V., Nelson, E. J., Daniel, R. F., Cinar, Y. Gippsland basin geosequestration: A potential solution for the latrobe valley brown coal co2 emissions. The Appea Journal, 2006, 46: 413.

Goodfellow, I., Bengio, Y., Courville, A., Bengio, Y. Deep learning. MIT press Cambridge, 2016.

Grinsztajn, L., Oyallon, E., Varoquaux, G. Why do tree-based models still outperform deep learning on tabular data? 2022. Available online: https://arxiv.org/abs/2207.08815 (accessed on March 2026)

Han, J., Kamber, M., Pei, J. Data mining: Concepts and. Techniques, Waltham: Morgan Kaufmann Publishers, 2012.

Han, W. S., McPherson, B. J., Lichtner, P. C., Wang, F. P. Evaluation of trapping mechanisms in geologic CO2 sequestration: Case study of SACROC northern platform, a 35-year CO2 injection site. American Journal of Science, 2010, 310: 282–324.

Helton, J. C., Davis, F. J. Latin hypercube sampling and the propagation of uncertainty in analyses of complex systems. Reliability Engineering & System Safety, 2003, 81: 23–69.

Honarpour, M. M., Nagarajan, N. R., Grijalba, A. C., Valle, M., Adesoye, K. Rock-Fluid Characterization for Miscible CO2 Injection: Residual Oil Zone, Seminole Field, Permian Basin, in: SPE Annual Technical Conference and Exhibition. Presented at the SPE Annual Technical Conference and Exhibition, SPE, Florence, Italy, 2010.

Hornik, K., Stinchcombe, M., White, H. Multilayer feedforward networks are universal approximators. Neural Networks, 1989, 2: 359–366.

Howell, K., Webb, N., Grigsby, N., Best, J. Reservoir architecture and heterogeneity of multistory fluvial sandstones of the Mississippian Cypress Formation, Illinois, USA: Implications for CO2 storage and EOR. In Conference Programme and Abstract Volume (pp. 149). University of Calgary, 2017.

Iglauer, S., Paluszny, A., Rahman, T., Zhang, Y., Wülling, W., Lebedev, M. Residual Trapping of CO_2 in an Oil-Filled, Oil-Wet Sandstone Core: Results of Three-Phase Pore-Scale Imaging. Geophysical Research Letters, 2019, 46: 11146–11154.

Koperna, G. J., Melzer, L. S., Kuuskraa, V. A. Recovery of Oil Resources from the Residual and Transitional Oil Zones of the Permian Basin. Presented at the SPE Annual Technical Conference and Exhibition, SPE, San Antonio, Texas, USA, 2006.

Lake, L. W., Johns, R., Rossen, B., Pope, G. A. Fundamentals of enhanced oil recovery. Society of Petroleum Engineers Richardson, TX, 2014.

Lee, J. H., Park, Y. C., Sung, W. M., Lee, Y. S. A Simulation of a Trap Mechanism for the Sequestration of CO_2 into Gorae V Aquifer, Korea. Energy Sources, Part A: Recovery, Utilization, and Environmental Effects, 2010, 32: 796–808.

Lee, K. J. Data-Driven Models to Predict Hydrocarbon Production From Unconventional Reservoirs by Thermal Recovery. Journal of Energy Resources Technology, 2020, 142: 123301.

Li, S., Zhang, Y. Model complexity in carbon sequestration: A design of experiment and response surface uncertainty analysis. International Journal of Greenhouse Gas Control, 2014, 22: 123–138.

Liberty, L. M., Yelton, J., Skurtveit, E., Braathen, A., Midtkandal, I., Evans, J. P. Regolith and host rock influences on CO2 leakage: Active source seismic profiling across the Little Grand Wash fault, Utah. International Journal of Greenhouse Gas Control, 2022, 119: 103742.

Lin, B., Tan, Z. How much impact will low oil price and carbon trading mechanism have on the value of carbon capture utilization and storage (CCUS) project? Analysis based on real option method. Journal of Cleaner Production, 2021, 298: 126768.

Lin, K., Wei, N., Zhang, Y., Ali, M., Chen, Q., Wang, W., Song, Z., Yin, Y., Vo Thanh, H. Advances in Machine-Learning-Driven CO2 Geological Storage: A Comprehensive Review and Outlook. Energy & Fuels, 2025, 39(28): 13315–13343.

Liu, B., Zhang, Y. CO_2 Modeling in a Deep Saline Aquifer: A Predictive Uncertainty Analysis Using Design of Experiment. Environmental Science & Technology, 2011, 45: 3504–3510.

Liu, T., Wu, P., Chen, Z., Li, Y. Review on Carbon Dioxide Replacement of Natural Gas Hydrate: Research Progress and Perspectives. Energy Fuels, 2022, 36: 7321–7336.

Longe, P., Danso, D. K., Gyamfi, G., Tsau, J. S., Alhajeri, M. M., Rasoulzadeh, M., Li, X., Barati, R. G. Predicting CO2 and H2 Solubility in Pure Water and Various Aqueous Systems: Implication for CO2–EOR, Carbon Capture and Sequestration, Natural Hydrogen Production and Underground Hydrogen Storage. Energies, 2024a, 17: 5723.

Longe, P., Davoodi, S., Mehrad, M., Wood, D. A. Robust machine-learning model for prediction of carbon dioxide adsorption on metal-organic frameworks. Journal of Alloys and Compounds, 2025a, 1010: 177890.

Longe, P., Davoodi, S., Mehrad, M., Wood, D. A. Combined Deep Learning and Optimization for Hydrogen-Solubility Prediction in Aqueous Systems Appropriate for Underground Hydrogen Storage Reservoirs. Energy Fuels, 2024b, 38: 22031–22049.

Longe, P., Molomjav, S., Barati, R., Tsau, J. -S., Musgrove, S., Villalobos, J., D'Erasmo, J., Alhajeri, M. M. Field-Scale Simulations of Water-Alternating-Gas Injection in Morrowan Fluvial Sandstones of Stewart Field, Kansas, Using Captured CO2 from an Ethanol Plant, Presented at the International Petroleum Technology Conference, IPTC, Dhahran, Saudi Arabia, 2024c.

Longe, P., Molomjav, S., Tsau, J. -S., Musgrove, S., Villalobos, J., D'Erasmo, J., Alhajeri, M. M., Barati, R. Techno-economic evaluation of CO2-EOR and carbon storage in a shallow incised fluvial reservoir using captured-CO2 from an ethanol plant. Geoenergy Science and Engineering, 2025b, 246: 213559.

Longe, P., Sanni, K., Okotie, S. New Production Rate Model of Wellhead Choke for Niger Delta Oil Wells. Journal of Petroleum Science and Technology, 2020, 10(4): 41–49.

Longe, P., Tsau, J. -S., Musgrove, S., Villalobos, J., D'Erasmo, J., Alhajeri, M. M., Barati, R. An Overview of Stewart Field Unit Project: A Field Case Study of CO2 Capture, Utilization, and Storage, Presented at the SPE Energy Transition Symposium, SPE, Houston, Texas, USA, 2024d.

Ma, W., Jafarpour, B., Qin, J. Dynamic characterization of geologic CO2 storage aquifers from monitoring data with ensemble Kalman filter. International Journal of Greenhouse Gas Control, 2019, 81: 199–215.

Mascle, M., Oisel, A., Munkerud, P. K., Ebeltoft, E., Lopez, O., Pryme, C., Youssef, S. CO2/Brine Relative Permeability Measurements at Reservoir Conditions: How to Reconciliate SS and USS Methods? Petrophysics – The SPWLA Journal of Formation Evaluation and Reservoir Description, 2025, 66: 26–43.

Massarweh, O., Abushaikha, A. S. CO2 sequestration in subsurface geological formations: A review of trapping mechanisms and monitoring techniques. Earth-Science Reviews, 2024, 253: 104793.

Mishra, S., Datta-Gupta, A. Applied Statistical Modeling and Data Analytics. Elsevier, 2018.

Mohaghegh, S. D. Smart Proxy Modeling: Artificial Intelligence and Machine Learning in Numerical Simulation. CRC Press, 2022.

Nabipour, N., Qasem, S. N., Mosavi, A., Shamshirband, S. Gaussian Process Prediction Model to Estimate Excess Adsorption Capacity of Supercritical CO2, 2020, Available online: https://doi.org/10.20944/preprints202002.0069.v1 (accessed on March 2026).

Nait Amar, M., Jahanbani Ghahfarokhi, A., Ng, C. S. W., Zeraibi, N. Optimization of WAG in real geological field using rigorous soft computing techniques and nature-inspired algorithms. Journal of Petroleum Science and Engineering, 2021, 206: 109038.

Olden, J. An accurate comparison of methods for quantifying variable importance in artificial neural networks using simulated data. Ecological Modelling, 2004, 178: 389-397.

Olden, J. D., Jackson, D. A. Illuminating the "black box": a randomization approach for understanding variable contributions in artificial neural networks. Ecological Modelling, 2002, 154: 135–150.

Panjalizadeh, H., Alizadeh, A., Ghazanfari, M., Alizadeh, N. Optimization of the WAG Injection Process. Petroleum Science and Technology, 2015, 33: 294–301.

Reisi, F., Mohammadzadeh, O., James, L. A. CO2/brine relative permeability estimation using effective

rock/fluid properties: A machine learning-based approach. Presented at 36th International Symposium for the Society of Core Analysts (SCA) , Abu Dhabi, UAE, 9-13 October 2023

Ren, B., Duncan, I. J. Reservoir simulation of carbon storage associated with CO2 EOR in residual oil zones, San Andres formation of West Texas, Permian Basin, USA. Energy, 2019, 167: 391–401.

Ren, B., Ren, S., Zhang, L., Chen, G., Zhang, H. Monitoring on CO2 migration in a tight oil reservoir during CCS-EOR in Jilin Oilfield China. Energy, 2016, 98: 108–121.

Roueché, J. N., Karacan, C. Ö. Zone identification and oil saturation prediction in a waterflooded field: Residual oil zone, East Seminole Field, Texas, USA, Permian Basin. Presented at the SPE Improved Oil Recovery Conference, SPE, 2018.

Ruprecht, C., Pini, R., Falta, R., Benson, S., Murdoch, L. Hysteretic trapping and relative permeability of CO2 in sandstone at reservoir conditions. International Journal of Greenhouse Gas Control, 2014, 27, 15–27.

Sedaghatinasab, R., Kord, S., Moghadasi, J., Soleymanzadeh, A. Relative Permeability Hysteresis and Capillary Trapping during CO2 EOR and Sequestration. International Journal of Greenhouse Gas Control, 2021, 106: 103262.

Shahkarami, A., Mohaghegh, S. Applications of smart proxies for subsurface modeling. Petroleum Exploration and Development, 2020, 47: 400–412.

Shwartz-Ziv, R., Armon, A. Tabular Data: Deep Learning is Not All You Need. Available online: https://arxiv.org/abs/2106.03253 (accessed on March 2026).

Specht, D. F. A general regression neural network. IEEE Transactions on Neural Networks, 1991, 2: 568–576.

Suykens, J. A. K., Vandewalle, J. Least Squares Support Vector Machine Classifiers. Neural Processing Letters, 1999, 9: 293–300.

Tahir, M. U., Guo, S. Preliminary Investigation of Fracture Behavior during Carbon Dioxide Fracturing of Natural Hydrogen Reservoir with Hard-Core Imperfections. Reservoir Science, 2026, 2: 34–51.

Trentham, R. C., Melzer, L. S. Case Studies of the ROZ CO_2 Flood and the Combined ROZ/MPZ CO_2 Flood at the Goldsmith Landreth Unit, Ector County, Texas. Using "Next Generation" CO_2 EOR Technologies to Optimize the Residual Oil Zone CO_2 Flood. Available online: https://www.osti.gov/servlets/purl/1224947/ (accessed on March 2026).

Van, S. L., Chon, B. H. Effective Prediction and Management of a CO2 Flooding Process for Enhancing Oil Recovery Using Artificial Neural Networks. Journal of Energy Resources Technology, 2018, 140: 032906.

Vo Thanh, H., Sugai, Y., Nguele, R., Sasaki, K. Robust optimization of CO2 sequestration through a water alternating gas process under geological uncertainties in Cuu Long Basin, Vietnam. Journal of Natural Gas Science and Engineering, 2020a, 76: 103208.

Vo Thanh, H., Sugai, Y., Sasaki, K. Application of artificial neural network for predicting the performance of CO2 enhanced oil recovery and storage in residual oil zones. Scientific Reports, 2020b, 10: 18204.

Wang, J., Zhang, Y., Xie, J. Influencing factors and application prospects of CO2 flooding in heterogeneous glutenite reservoirs. Scientific Reports, 2020, 10: 1839.

Webb, N. D. Studies and field data on a Cypress sandstone ROZ in Illinois. Presented at the CO2 & ROZ Conference, Midland, Texas, USA, 2017.

Wilday, J., Wardman, M., Johnson, M., Haines, M. Hazards from carbon dioxide capture, transport and storage. Process Safety and Environmental Protection, 2011, 89: 482–491.

Wu, J., Ansari, U. From CO2 Sequestration to Hydrogen Storage: Further Utilization of Depleted Gas Reservoirs. Reservoir Science, 2025, 1: 19–35.

Xiao, Z., Shen, B., Yang, J., Yang, K., Zhang, Y., Yang, S. Deep Learning Framework for Accurate Static and Dynamic Prediction of CO2 Enhanced Oil Recovery and Storage Capacity. Processes, 2024, 12: 1693.

Yang, Y., Huang, F., Kang, S. Mechanism of Penetration Rate Improvement in Hot Dry Rock Under the Coupling of Impact Load and Confining Pressure Release. Reservoir Science, 2026, 2: 52–64.

Yao, P., Yu, Z., Zhang, Y., Xu, T. Application of machine learning in carbon capture and storage: An in-depth insight from the perspective of geoscience. Fuel, 2023, 333: 126296.

You, J., Ampomah, W., Sun, Q. Development and application of a machine learning based multi-objective optimization workflow for CO2-EOR projects. Fuel , 2020, 264: 116758.

Zhang, K., Lau, H. C. Regional opportunities for CO2 capture and storage in Southeast Asia. International Journal of Greenhouse Gas Control, 2022, 116: 103628.